

V. Petoukhov · M. Claussen · A. Berger · M. Crucifix
M. Eby · A. V. Eliseev · T. Fichefet · A. Ganopolski
H. Goosse · I. Kamenkovich · I. I. Mokhov
M. Montoya · L. A. Mysak · A. Sokolov · P. Stone
Z. Wang · A. J. Weaver

EMIC Intercomparison Project (EMIP–CO₂): comparative analysis of EMIC simulations of climate, and of equilibrium and transient responses to atmospheric CO₂ doubling

Received: 4 February 2005 / Accepted: 2 May 2005 / Published online: 23 July 2005
© Springer-Verlag 2005

Abstract An intercomparison of eight EMICs (Earth system Models of Intermediate Complexity) is carried out to investigate the variation and scatter in the

results of simulating (1) the climate characteristics at the prescribed 280 ppm atmosphere CO₂ concentration, and (2) the equilibrium and transient responses to CO₂ doubling in the atmosphere. The results of the first part of this intercomparison suggest that EMICs are in reasonable agreement with the present-day observational data. The dispersion of the EMIC results by and large falls within the range of results of General Circulation Models (GCMs), which took part in the Atmospheric Model Intercomparison Project (AMIP) and Coupled Model Intercomparison Project, phase 1 (CMIP1). Probable reasons for the observed discrepancies among the EMIC simulations of climate characteristics are analysed. A scenario with gradual increase in CO₂ concentration in the atmosphere (1% per year compounded) during the first 70 years followed by a stabilisation at the 560 ppm level during a period longer than 1,500 years is chosen for the second part of this intercomparison. It appears that the EMIC results for the equilibrium and transient responses to CO₂ doubling are within the range of the corresponding results of GCMs, which participated in the atmosphere-slab ocean model intercomparison project and Coupled Model Intercomparison Project, phase 2 (CMIP2). In particular EMICs show similar temperature and precipitation changes with comparable magnitudes and scatter across the models as found in the GCMs. The largest scatter in the simulated response of precipitation to CO₂ change occurs in the subtropics. Significant differences also appear in the magnitude of sea ice cover reduction. Each of the EMICs participating in the intercomparison exhibits a reduction of the strength of the thermohaline circulation in the North Atlantic under CO₂ doubling, with the maximum decrease occurring between 100 and 300 years after the beginning of the transient experiment. After this transient reduction, whose minimum notably varies

V. Petoukhov (✉) · M. Claussen · A. Ganopolski
Potsdam Institute for Climate Impact Research,
Germany
E-mail: Vladimir.Petoukhov@pik-potsdam.de
Fax: +49-331-2882570

A. Berger · M. Crucifix · T. Fichefet · H. Goosse
Institut d'Astronomie et de Géophysique Georges Lemaître,
Université Catholique de Louvain, Belgium

Present address: M. Crucifix
Hadley Centre for Climate Prediction and Research,
Met Office, Exeter, Devon, UK

M. Eby · A. J. Weaver
School of Earth and Ocean Sciences,
University of Victoria, Canada

A. V. Eliseev · I. I. Mokhov
A.M.Obukhov Institute of Atmospheric Physics,
Russian Academy of Sciences, Russia

I. Kamenkovich
Department of Atmospheric Sciences,
Joint Institute for the Study of the Atmosphere and the Oceans,
University of Washington, Seattle, USA

M. Montoya
Dpto. Astrofísica y Ciencias de la Atmosfera,
Facultad de Ciencias Físicas,
Universidad Complutense de Madrid, Spain

L. A. Mysak · Z. Wang
Department of Atmospheric and Oceanic Sciences,
McGill University, Montreal, Canada

A. Sokolov
Joint Program on the Science and Policy of Global Change,
Massachusetts Institute of Technology, USA

P. Stone
Department of Earth, Atmosphere and Planetary Science, Massa-
chusetts Institute of Technology, USA

from model to model, the strength of the thermohaline circulation increases again in each model, slowly rising back to a new equilibrium.

1 Introduction

Current studies in the field of climate modelling are carried out using tools of different complexity, from the simplest conceptual models up to the highly sophisticated 3-D General Circulation Models (GCMs). Earth system Models of Intermediate Complexity (EMICs, Claussen et al. 2002) are a category of climate models, which occupy an intermediate position in the spectrum of climate system models with respect to the degree of complexity in the description of climatic processes and not infrequently include more climatic variables than coupled GCMs. A specific feature of EMICs, which differentiates them from other categories of climate models, is that they comprise, in an interactive mode, all the basic components of the global climate system, including the atmosphere, ocean, cryosphere (with sea ice, continental ice and permafrost areas accounted for) and land masses (with different soil/vegetation and land-use patterns), over a very wide range of temporal scales, from a season to hundred thousand and even million years. This allows one to explore the complex behaviour of the Earth's climate system as an integrated multi-component system with multi-scale, nonlinearly coupled processes.

EMICs are now widely employed in the analysis of a variety of climate mechanisms and feedbacks (Opsteegh et al. 1998; Rahmstorf and Ganopolski 1999; Goosse et al. 2001; Wang and Mysak 2002; Eliseev and Mokhov 2003) as well as in the assessment of future climate projections (Alcamo et al. 1996; Prinn et al. 1999; Ganopolski et al. 2001; Demchenko et al. 2002; Mokhov et al. 2002, 2005; Ewen et al. 2004) and in paleoclimate reconstructions (Stocker et al. 1992; Ganopolski et al. 1998; Weaver et al. 1998; Crucifix et al. 2002; Renssen et al. 2002; Schmittner et al. 2002). EMICs represent a compromise between the integral approach to the study of the Earth's climate—which means the incorporation into the models of almost all the climate components and their interactions—and the fast turn-around time of integration. This last feature makes EMICs one of the more promising instruments for exploring the Earth's climate evolution on a wide range of temporal and spatial scales. In this way, EMICs have to be used alongside with other types of climate models, specifically modern global coupled ocean-atmosphere GCMs, which include interactive sea ice. These latter state-of-the-art climate models provide the most physically based climate simulations and, unlike EMICs, describe explicitly, and not in a parameterised form, the intra-seasonal (e.g. weather) processes. Furthermore, the GCM approach is the only way to downscale the produced climatic information and therefore is one of the reasons for keeping GCMs more and more detailed.

Historically, the present-day EMICs stem from a class of the statistical-dynamical climate models (see, e.g. Saltzman and Vernekar 1971, 1972; Stone 1972; Petoukhov and Feygel'son 1973). These latter models explicitly described long-term atmospheric statistical characteristics, e.g. monthly or longer normals and normal variances. An excellent review of statistical-dynamical climate models—which, by the way, were the result of the modification and generalisation of Budyko-Sellers-type energy balance models—is given in Saltzman (1978). The first prototypes for the modern EMICs that already included—although in a simplified form—all the basic coupled components of the Earth's climate system (except for biosphere) were proposed in Petoukhov (1980), Chalikov and Verbitsky (1984), Gallée et al. (1991) and Petoukhov (1991). The models of Petoukhov (1980) and Chalikov and Verbitsky (1984) involved, in particular, ice mass balance equations. [Later on, Verbitsky and Chalikov (1986) extended their model by including the asthenosphere compartment, in order to treat some of the ultra-long climate processes.] The Gallée et al. (1991) and Petoukhov (1991) models contained modules of the continental ice sheets, with different degrees of detail as to the ice-sheet processes. In Oglesby and Saltzman (1990), the above-mentioned zonally averaged Saltzman and Vernekar (1972) statistical-dynamical climate model has been extended to accounting for some important oceanic processes, except for ocean dynamics. Stocker et al. (1992) and Harvey (1992), however, developed climate models which incorporated fully coupled zonally averaged dynamical ocean and atmospheric components.

Unlike in the case of GCMs, there has not yet been any intercomparison study of EMICs, a process which could help to substantially upgrade the performance of these models and raise the degree of confidence of their results. This paper is the first attempt to fill this gap in the literature. In Sect. 2, the results are shown of the intercomparison of eight EMICs (see Tables 1, 2, 3, 4) on modelling the climate with (pre-industrial) 280 ppm atmospheric CO₂ concentration (hereafter referred to as the “Equilibrium 1×CO₂” run 1). In Sect. 2, EMIC results are also compared with the relevant present-day observational data and, wherever possible, with results obtained from GCMs which took part in the Atmospheric Model Intercomparison Project (AMIP, see Gates et al. 1999) and the first phase (simulation of the present-day climate) of the Coupled Model Intercomparison Project (CMIP1, see Covey et al. 2000, 2003; Lambert and Boer 2001). Thirty one atmospheric general circulation models (AGCMs), which participated in the AMIP, simulated the evolution of the climate during the decade 1979–1988, under the observed monthly average sea surface temperature and sea ice and a prescribed atmospheric CO₂ concentration and solar constant (Gates et al. 1999). In Lambert and Boer (2001), the climates are intercompared in fifteen coupled atmosphere-ocean-sea ice general circulation models (AOGCMs) that participated in the CMIP1. Covey et al.

Table 1 List of EMICs participating in the intercomparison (Continued in Tables 2, 3, 4)^a

Model key references	Basic module structure	Interactive variables	Specified variables
CLIMBER-2 Petoukhov et al. (2000), Ganopolski et al. (2001)	2.5-D (ϕ, λ , multi-layer in z coordinate, with parameterised vertical structure) statistical-dynamical (SD) atmospheric module (AM); 2-D (ϕ, z) zonally averaged 3-basin oceanic module (OM); thermodynamic sea ice module (SIM) with the bulk advection and sea ice dynamics; 3-D polythermal ice sheet module (ISM); 2-layer soil moisture module (SMM); VECODE (Brovkin et al. 1997) as the vegetation/land-cover module (VLM)	Large-scale long-term T^a , q and D^a , 2-type 1-layer C ; F^{a}_{sh} , F^{a}_{sz} , $(Y^a_s)^2$; T^o , S , D^o ; H^{is} , n^{is} , T^{is} , D^{is} ; H^{ic} , T^{ic} , D^{ic} ; W_s ; 3-type V_f ; C^o_c ; C^l_c	GHGs (except for CO ₂); A_e

^a In Tables 1, 2, 3, 4, T^a (T^o , T^{is} , T^{ic}) and D^a (D^o , D^{is} , D^{ic})-atmospheric (oceanic, sea ice, continental ice) temperature and dynamics, q -atmospheric specific humidity, C -cloudiness, F^{a}_{sh} (F^{a}_{sz}) and $(Y^a_s)^2$ -atmospheric eddy-ensemble horizontal (vertical) fluxes and variances, S -oceanic salinity, H^{is} (H^{ic})-sea (continental) ice thickness, n^{is} -sea ice concentration (the percentage of area covered by ice), W_s -soil moisture, V_f -vegetation fraction, C^o_c (C^l_c)-oceanic (terrestrial) carbon content, GHGs (A_e)- atmospheric greenhouse gas(aerosol) concentrations

Table 2 List of EMICs participating in the intercomparison (continued from Table 1)

Model key references	Basic module structure	Interactive variables	Specified variables
CLIMBER-3 α Montoya et al. (2004)	Modified version of CLIMBER-2, with AM, ISM, SMM and VLM from CLIMBER-2, 3-D general circulation model (MOM-3) as OM, ISIS (Fichefet and Morales-Maqueda 1997) as SIM, and a spatial resolution higher than in CLIMBER-2	Large-scale long-term T^a , q and D^a , 2-type 1-layer C ; F^{a}_{sh} , F^{a}_{sz} , $(Y^a_s)^2$; T^o , S , D^o ; H^{is} , n^{is} , T^{is} , D^{is} ; H^{ic} , T^{ic} , D^{ic} ; W_s ; 3-type V_f ; C^o_c ; C^l_c	GHGs (except for CO ₂); A_e
EcBilt-CLIO Goosse et al. (2001)	3-D quasi-geostrophic (QG) general circulation AM; 3-D general circulation OM; comprehensive-dynamic thermodynamic SIM with the sea-ice rheology allowed for; 3-D polythermal ISM; bucket-type SMM; VECODE as VLM	T^a , q , D^a ; T^o , S , D^o ; H^{is} , n^{is} , T^{is} , D^{is} ; H^{ic} , T^{ic} , D^{ic} ; W_s ; 3-type V_f ; C^o_c ; C^l_c	present-day climatological C ; GHGs (except for CO ₂); no A_e
IAP RAS Petoukhov et al. (1998), Mokhov et al. (2002)	2.5-D (ϕ, λ , multi-layer in z coordinate) SD AM, with 7-layer stratospheric sub-module; nonzonal 4-layer OM; diagnostic thermodynamic SIM with no sea ice advection and dynamics; mass/energy-balance ISM; BATS (Dickinson et al. 1986) as SMM	Large-scale long-term T^a , q and D^a , 2-type 3-layer C ; F^{a}_{sh} , F^{a}_{sz} , $(Y^a_s)^2$; T^o , D^o ; H^{is} , T^{is} , n^{is} , H^{ic} , T^{ic} ; W_s	S ; V_f ; GHGs; A_e

(2003) reported on the results from the extended set of 18 AOGCMs which took part in the CMIP1.

In Sect. 3 of this paper, the results of modelling the equilibrium (“Equilibrium 2×CO₂” run 3, with 560 ppm atmospheric carbon dioxide concentration) response of the same eight EMICs to a CO₂ doubling in the atmosphere are shown. In Sect. 4, the results of the transient (“Transient 2×CO₂” run 2, with 1% per year increasing atmospheric carbon dioxide concentration) and the combined “Transient” and “Equilibrium” 2×CO₂ runs 2

and 3 in the aforementioned eight EMICs are described. The EMIC performance is compared with that of the GCMs that were analysed, basically, in the reviews by Covey et al. (2000, 2003) and Le Treut and McAvaney (2000). Covey et al. (2000) display, in particular, equilibrium globally averaged mean annual surface air temperature warming due to doubled atmospheric CO₂ in seventeen coupled AOGCMs that participated in the second phase of CMIP (1% per year increasing atmospheric carbon dioxide simulations, CMIP2), while in Le

Table 3 List of EMICs participating in the intercomparison (continued from Tables 1, 2)

Model key references	Basic module structure	Interactive variables	Specified variables
MIT Prinn et al. (1999), Kamenkovich et al. (2002)	2-D (ϕ, z) SD AM with 2-D (ϕ, z) atmosphere chemistry sub-module; 3-D OM; thermodynamic SIM with no sea ice advection and dynamics; simplified energy-balance ISM; SMM	T^a, q , 2-type multi-layer $C, D^a; F^a_{sh}, F^a_{sz}, (Y^a_s)^2$; $T^o, S, D^o; H^{is}, T^{is}, T^{ic}$; $W_s; C^o_c; C^l_c; GHGs; A_e$	$H^{ic}; V_f$
MoBidiC Crucifix et al. (2002)	2-D (ϕ, z) QG 2-layer AM with two(Hadley)-cell mean meridional circulation; 2-D (ϕ, z) zonally averaged 3-basin OM; thermodynamic SIM with the bulk advection and sea ice dynamics; 1-D (ϕ) with plastic assumption in zonal direction isothermal ISM; SMM; VECODE as VLM	$D^a, T^a, q; F^a_{sh}; T^o, S, D^o$; $H^{is}, n^{is}, T^{is}, D^{is}; H^{ic}, T^{ic}, D^{ic}$; W_s ; 3-type V_f	1-layer seasonal C ; GHGs; A_e
MPM Wang and Mysak (2000, 2002)	1.5-D (ϕ, λ) energy-moisture balance (EMB) AM with land/ocean boxes; 2-D (ϕ, z) 3-basin OM; thermodynamic SIM with prescribed advection (but note, no Arctic ocean in the model); 1-D (ϕ) with plastic assumption in zonal direction isothermal ISM; SMM; VECODE as VLM	$T^a, q, D^a; F^a_{sh}; T^o, S, D^o$; $H^{is}, n^{is}, T^{is}; H^{ic}, T^{ic}, D^{ic}; W_s$	Albedo and absorption of the atmosphere; D^{is} ; GHGs; no A_e

Treut and McAvaney (2000) an intercomparison is carried out to investigate the scatter in the simulated equilibrium response to a CO₂ doubling in 11 AGCMs coupled to a slab ocean. Covey et al. (2003) summarised the results from the latest versions of 18 coupled AOGCMs participating in CMIP2.

Specifically, in this paper the scatter of the EMIC results when modelling a particular climate variable is compared with the range of GCM results for the same variable, which we define as a continuum of values for this variable enclosed by the minimum and maximum values produced by a set of GCMs that is used for the comparison with EMIC results. In some special cases, the EMIC results exhibited in Sects. 2, 3, and 4 are compared with individual GCM data presented in the reports of the Intergovernmental Panels on Climate Change (IPCC 1990, 1995, 2001).

In Claussen et al. (2002) a table is given (see Table 2 from their cited paper) of the climate system interactive

components implemented into the EMICs under consideration. For a better understanding and interpretation of the EMIC results displayed below in Sects. 2, 3, and 4 of this paper, Tables 1, 2, 3, and 4 illustrate some specific features of the design of the later versions of the EMICs participating in the intercomparison. From these tables it should be noted that all EMICs include the water vapour, surface (in particular, sea ice) albedo and surface temperature feedbacks—according to Colman et al. (2001) nomenclature—and contain the soil moisture as an interactive climate component. Not all EMICs (e.g. CLIMBER-3 α , EcBilt-CLIO, IAP RAS, MIT and UVic) use a zonally averaged ocean model. The CLIMBER-2, CLIMBER-3 α , IAP RAS and MIT models include interactive cloudiness and contain most of the cloud feedbacks mentioned in Colman et al. (2001) (i.e., the cloud amount, height, physical thickness and convective cloud fraction feedbacks), while CLIMBER-2, CLIMBER-3 α , EcBilt-CLIO, IAP RAS, MIT

Table 4 List of EMICs participating in the intercomparison (continued from Tables 1, 2, 3)

Model key references	Basic module structure	Interactive variables	Specified variables
UVic Weaver et al. (2001)	Modular structure with multi-optional description of the model subcomponents; 2-D (ϕ, λ) EMB AM with a diffusion scheme for the atmosphere heat transport; 3-D OM; highly sophisticated SIM; 3-D polythermal ISM; SMM; VLM	T^a, q , atmospheric surface winds; T^o, S, D^o ; $H^{is}, n^{is}, T^{is}, D^{is}$; $H^{ic}, T^{ic}, D^{ic}; W_s, V_f; C^o_c; C^l_c$	Atmospheric wind data for the transport of water vapour; atmosphere/cloud albedo and absorption; GHGs (except for CO ₂); no A_e

and MoBidiC capture the lapse rate feedback (see Colman et al. 2001). All EMICs participating in the intercomparison, except for IAP RAS, comprise an interactive vegetation/land cover module, in their latest version.

In the context of the specific features of the EMICs given in Tables 1, 2, 3, and 4, it should also be mentioned that the UVic model is highly modular with numerous options for various subcomponent models and physical parameterisations. The sea ice module of UVic incorporates an elastic-viscous-plastic rheology representation of dynamics and ice/snow thermodynamics. Two different land surface modules are implemented in the model: one is a simple bucket model (Matthews et al. 2003), which is used in this paper, and another is a simplified one-layer version of the Hadley Centre MOSES surface scheme. Although not utilised in the presented runs, the UVic model also includes, in its latest version, an interactive vegetation module [the Hadley Centre dynamic global vegetation module (TRIFFID), see Cox et al. (2000); Cox (2001); Meissner et al. (2003)], and TEOCARD (TRIFFID and Ocean Chemistry/Biology model). CLIMBER-3 α employs MOM-3 (GFDL, Princeton) as the oceanic module, with a free upper boundary condition in the oceanic dynamical sub-module (Levermann et al. 2005), and ISIS (Ice and Snow Interface model, Fichfet and Morales-Maqueda 1997) as the sea ice module.

We note that, for a higher consistency with each other and GCMs in the setup of the climate simulations, all the EMICs participating in the intercomparison (except for MPM) conducted the above-mentioned runs 1 to 3 with a specified (present-day) vegetation/land cover mask. We note, however, that in the current version of the MPM, a modified form of VECODE (Brovkin et al. 1997) is used as the vegetation/land cover module. Also, in all EMICs participating in the intercomparison the present-day solar constant and land ice mask were specified in the runs 1 to 3.

In the Conclusions, the basic implications for the results of the intercomparison are presented. The strengths and weaknesses of EMICs, with respect to the description of individual climate variables, mechanisms and feedbacks, are analysed, as well as the possible lines of attack on the unsolved problems.

2 “Equilibrium 1 \times CO₂” run 1 with pre-industrial CO₂ concentration in the atmosphere

In this section, the intercomparison of the EMIC results are presented for the variables averaged over the last 10 years of the run that is described in the Introduction as “Equilibrium 1 \times CO₂” run 1, under constant (pre-industrial) 280 ppm atmosphere CO₂ concentration. The duration of the run 1 was long enough to reach an “equilibrium”, in all the EMICs.

The reason for comparing the results of simulations of the pre-industrial climate with 280 ppm atmosphere CO₂ concentration in all models is to avoid the uncertainty in the setup of the experiments in different models that usually occurs in the simulations of the present-day climate. An example of such a problem occurred in the CMIP1 project where the prescribed atmosphere CO₂ concentration in the control run for the present-day climate varied from model to model over a wide range in order to get as close an agreement with a broad set of the present-day observational data as possible (Gates et al. 1992; Covey et al. 2003). Meanwhile, the scatter in the results of the above-mentioned control runs in different CMIP1 GCMs, e.g. for the present-day zonally averaged surface air temperatures (see Fig. 1a, b), is in some latitudinal belts far beyond the values of the observed trends of these characteristics from the pre-industrial times to present.

2.1 Surface air temperature

The curves in Fig. 1a, b show the latitudinal distribution of the zonally averaged surface air temperature (SAT) for DJF (panel a) and JJA (panel b) simulated by eight EMICs. In the same figure, for comparative purposes, the observational curves merged from the closely patched data of Jennings (1975), Jones (1988), Schubert et al. (1992), da Silva et al. (1994), and Fiorino (1997) are also shown for the present-day climate conditions. From Fig. 1a, b we note that the results of EMICs are in a rather good agreement with each other, except for the polar latitudes in the Northern (NH) and Southern (SH) Hemisphere, where the results from the total set of the AMIP (with prescribed sea surface temperature and sea ice) and CMIP1 (with coupled oceanic, atmospheric and sea ice modules) GCMs for the present-day climate conditions also show a marked scatter and deviate noticeably from the observed values. As seen from Fig. 1a, b for both seasons and in all the latitudinal belts, the scatter of EMIC curves, on the whole, is not larger than the range of GCM results (as defined above in the Introduction) for the AMIP and CMIP1 GCMs. We note that the “present-day” CO₂ concentrations in the CMIP1 GCMs varied over a wide range, from 290 to 345 ppm (Gates et al. 1992; Covey et al. 2003). In general, the latitudinal distributions of the EMIC simulated surface air temperatures in the NH for DJF exhibit a larger scatter than those for JJA. This is basically due to differences in the modelled annual cycle of sea ice cover in the presented EMICs, part of which (see Tables 1, 2, 3, 4) include zonal oceanic modules (for details, see subsection “Sea ice area” in this section).

2.2 Planetary albedo

Figure 1c, d shows the DJF (panel c) and JJA (panel d) pole-to-pole distribution of the zonally averaged

Table 5 Maximum value of the North Atlantic overturning streamfunction (MAOSF, in Sv) from five observationally based estimates, and from seven GCMs for the present-day climate condition and seven EMICs for the “Equilibrium 1×CO₂” run 1

Data/model	MAOSF
Schmitz and McCartney (1993)	13
Dickson and Brown (1994)	13
Schmitz (1995)	14
Ganachaud and Wunsch (2000)	15
Talley et al. (2003)	18
GFDL, Manabe and Stouffer (1988)	12
University of Sydney GCM, England (1993)	18
Hamburg LSG GCM, Maier-Reimer et al. (1993)	22
GFDL, Manabe and Stouffer (1999)	16
GFDL LVD, Manabe and Stouffer (1999)	28
CCSR GCM, Oka et al. (2001)	18
CGCM2, Kim et al. (2002)	12
CLIMBER-2	21
CLIMBER-3 α	12
EcBilt-CLIO	17
MIT	25
MoBidiC	19
MPM	19
UVic	17

Table 6 North Atlantic annual mean heat flux F_{hm} (in PW) at the latitude ϕ_{hm} of its maximum and the freshwater flux F_{fw} (in Sv) in the Atlantic Ocean at 30°S in EMICs for the “Equilibrium 1×CO₂” run 1

Model	F_{hm}	ϕ_{hm}	F_{fw}
CLIMBER-2	1.10	20°N	0.25
CLIMBER-3 α	0.80	15°N	0.19
EcBilt-CLIO	0.71	25°N	0.55
IAP RAS	-	-	0.25
MIT	1.06	16°N	0.63
MoBidiC	0.93	25°N	0.30
MPM	0.96	25°N	0.30
UVic	0.73	22.5°N	0.18

planetary albedo in the EMICs, along with the observational data on this characteristic from Campbell and Vonder Haar (1980) and Harrison et al. (1990). Essentially at all the latitudes, the results of the EMICs are within the range of GCM results obtained in the AMIP GCMs (see Fig. 1c, d); however, the MPM curve is

somewhat “flat” in the middle latitudes of the SH in JJA, apparently, due to the prescribed symmetric (with respect to the equator) latitudinal distribution of the atmospheric albedo, see Table 3 and Wang and Mysak (2000). Also, the MIT model slightly underestimates the planetary albedo in the middle and subpolar latitudes of the NH for the same season, which could be a consequence of somewhat low values of the total cloud amount and sea ice cover for this season in the model (see Fig. 4a, b, Table 7 below).

2.3 Outgoing longwave radiation

In Fig. 1e, f, the latitudinal distribution of the zonally averaged outgoing longwave radiation (OLR) in the EMICs is shown in comparison with data from Harrison et al. (1990) and the merged data from Campbell and Vonder Haar (1980) and Hurrell and Campbell (1992). Obviously, CLIMBER-2, CLIMBER-3 α , EcBilt-CLIO, MIT and MoBidiC resolve the bimodal structure of OLR in the tropical region for both the boreal winter (panel e) and summer (panel d) rather successfully. This structure is associated with the latitudinal distribution in the area of the “effective cloud top” temperature of the tropical cloud system which, to a first approximation, follows the latitudinal structure of the vertical motions in the Hadley cells in the NH and SH. [Let us recall that the climatological mean annual (seasonal) cloudiness is prescribed in EcBilt-CLIO (MoBidiC), see Tables 2 and 3]. This OLR structure is less pronounced in the IAP RAS model. It is not seen in UVic and MPM models, since there is no explicit module of the cloudiness in these two EMICs (see Tables 3, 4 and the accompanying text to Fig. 1c, d above). In regard to the overall latitudinal structure of OLR, the EMICs by and large match the observed data with reasonable accuracy and fall within the limits of the range of GCM results for the AMIP climate models (see Fig. 1e, f).

2.4 Precipitation

Being one of the most important climate variables, precipitation (P) affects—along with the temperature,

Table 7 Present-day NH and SH sea ice cover from the observationally based estimates (Robock 1980; Ropelewski 1989) and sea ice areas from seven EMICs for the “Equilibrium 1×CO₂” run 1 (in 10⁶ km²)

	NHI, DJF	NHI, JJA	NHI _{max}	NHI _{min}	SHI, DJF	SHI, JJA	SHI _{max}	SHI _{min}
Robock (1980)	13.3	8.8	14.1	7.2	6.9	16.3	19.1	4.3
Ropelewski (1989)	13.4	11.3	15.2	8.0	11.7	15.9	20.7	6.0
CLIMBER-2	12.8	8.5	16.5	4.2	8.1	16.6	18.2	5.1
CLIMBER-3 α	12.2	4.3	14.3	1.9	14.6	28.8	30.9	9.2
EcBilt-CLIO	14.2	9.4	15.3	8.6	4.6	15.8	16.4	4.0
MIT	9.6	6.4	9.9	4.6	8.0	13.1	13.7	3.2
MoBidiC	15.0	4.0	15.6	0.3	1.4	10.9	13.9	0.03
MPM					11.3	14.2	16.8	9.4
UVic	14.1	7.5	15.2	3.9	6.0	18.6	21.7	3.0

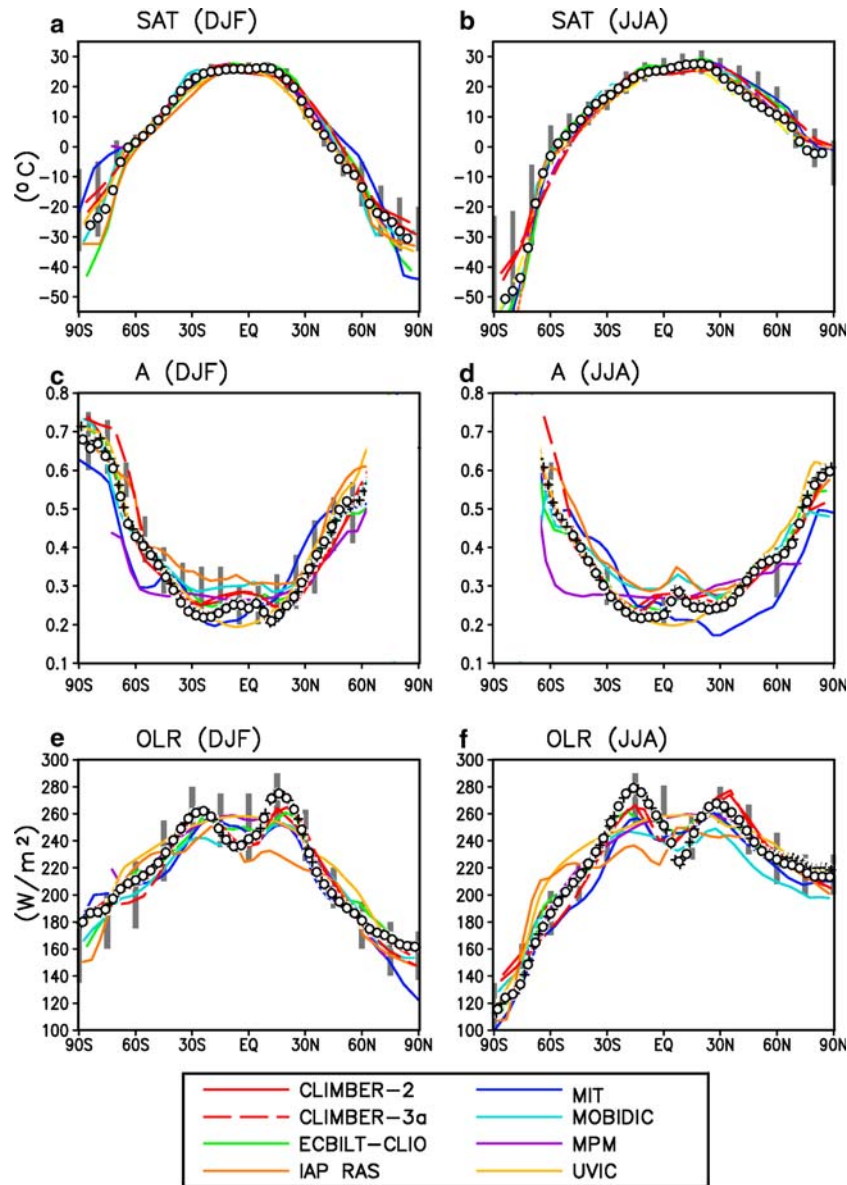


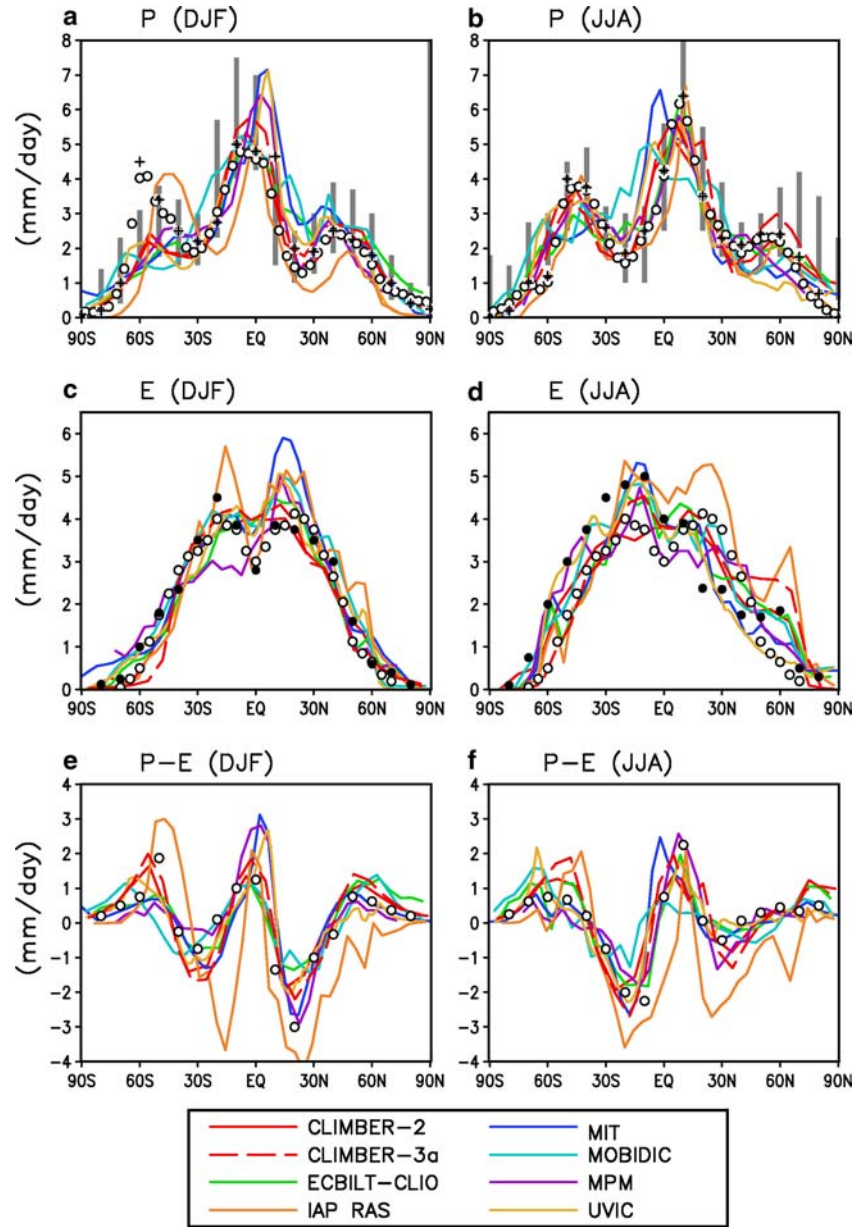
Fig. 1 Latitudinal distribution of simulated zonally averaged surface air temperature (SAT, in °C) (a, b), planetary albedo (A, as a fraction of unity) (c, d) and outgoing longwave radiation (OLR, in W/m²) (e, f) in the EMICs for DJF (a, c, e) and JJA (b, d, f). In a and b the present-day observational data on SAT as merged from Jennings (1975), Jones (1988), Schubert et al. (1992), da Silva et al. (1994) and Fiorino (1997) are shown by open circles; the vertical bars designate the range of GCM results (as defined in the Introduction section) in the simulations of the present-day SAT in a full set of GCMs that took part in the AMIP and CMIP1 intercomparison projects analysed in Gates et al. (1999) and Lambert and Boer (2001), respectively. In c and d, the present-day observational data on A are displayed from Campbell and Vonder

Haar (1980) (open circles) and Harrison et al. (1990) (crosses); the vertical bars in c and d label the range of GCM results in the simulated present-day A for DJF and JJA in the NCAR, GISS, CCC, GFHI and UKHI climate models which took part in the AMIP, as displayed in IPCC (1990). In panels e and f, the observational data on OLR are depicted from Harrison et al. (1990) (crosses) and the merged data from Campbell and Vonder Haar (1980) and Hurrell and Campbell (1992) (open circles); the range of GCM results for OLR in e and f is marked by the vertical bars as derived from the results for the AMIP models presented in IPCC (1995) and Gates et al. (1999). [See legend to the figure for EMIC identification.]

soil moisture and radiation—the life cycle of the vegetation patterns over the land, and—along with the evaporation and runoff—the freshwater flux to the oceans. This latter quantity is recognised to be one of the major influences on the global oceanic thermohaline circulation. The majority of the EMICs (see Fig. 2a, b) satisfactorily mimics the general structure of the

observed zonally averaged *P* from Jäger (1976) and Xie and Arkin (1997), with the local maxima and minima, respectively, in the middle latitudes and subtropics of both hemispheres and the absolute maximum in the tropics. It is worth noting that there is a pronounced discrepancy between two sets of observational data at the middle latitudes of the SH for DJF and JJA. For

Fig. 2 Zonally averaged precipitation (P , in mm/day) (a, b), evaporation (E , in mm/day) (c, d), and precipitation minus evaporation ($P-E$, in mm/day) (e, f) in the EMICs as a function of latitude for DJF (a, c, e) and JJA (b, d, f). In a and b, the observational data on P are shown from Jäger (1976) (crosses) and Xie and Arkin (1997) (open circles); the vertical bars mark the range of GCM results as derived from the entire set of the results of the AMIP (Gates et al. 1999) and CMIP1 (Lambert and Boer 2001) intercomparison projects. In c and d, the empirical data on E are depicted from Kessler (1968) (open circles) and NCEP-NCAR reanalysis given on <http://iridl.ldeo.columbia.edu/SOURCES/.NOAA/.NCEP-NCAR/.CDAS-1/.MONTHLY> websites [see also Kalnay et al. (1996)] (solid circles). In e and f, the empirical data on $P-E$ are displayed from Peixoto and Oort (1983) (open circles). [See legend to the figure for EMIC identification.]

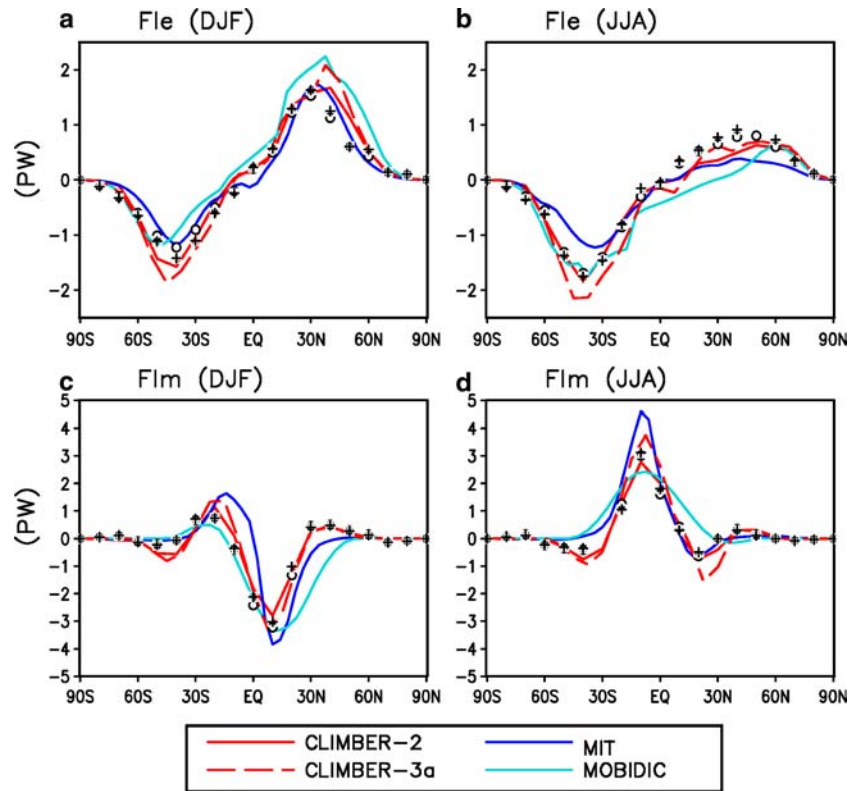


most latitudes the results of all the EMICs are within the range of GCM results inherent in the entire set of the AMIP and CMIP1 models (see Fig. 2a, b), except for middle latitudes of the NH where the IAP RAS model gives somewhat low values of P for DJF.

The underestimation of the amount of precipitation in the IAP RAS model in the middle latitudes of the NH in winter is attributed to the relatively low value of the total cloud amount in the model for this season in the NH (see Fig. 4a, b below). Basically, this is caused by some overestimation (underestimation) of the intensity of the descending (ascending) branch of the Hadley (Ferrel) cell in the NH winter in the IAP RAS model, as well as by the underestimation of the swing of the seasonal variations of the synoptic activity in the model. In this context, the principle background problem is the

adequate simulation in the EMICs (e.g. in CLIMBER-2, CLIMBER-3 α , IAP RAS and MIT) of a delicate linkage among the spatial and seasonal distributions of the atmosphere angular momentum, heat and moisture fluxes, large-scale free and forced convection patterns and the atmosphere temperature and moisture. The above-mentioned distributions of the atmospheric temperature and moisture regulate, in particular, the static stability parameter of the atmosphere and the horizontal and vertical gradients of the (virtual) potential temperature. These two enter the parameterisation formulas for the synoptic-scale eddy momentum, heat and moisture fluxes which strongly influence, specifically, the intensity of the atmospheric mean meridional circulation cells in the above-mentioned EMICs. In this context, we note also the second maximum of P in the NH tropics for

Fig. 3 Latitudinal distribution of the vertically and longitudinally integrated fluxes of latent heat (in PW) in CLIMBER-2, CLIMBER-3 α , the MIT model and MoBidiC by eddies (F_{le}) (a, b) and due to the mean meridional circulation (F_{lm}) (c, d) for DJF (a, c) and JJA (b, d), compared with the empirical data on (F_{le}) and (F_{lm}) from Oort and Rasmusson (1971) (open circles) and Peixoto and Oort (1983) (crosses). [See legend to the figure for EMIC identification]



DJF and JJA, and in the SH tropics for JJA in the MoBidiC model; this could be attributed to a special scheme of calculation of the “macroturbulent diffusion” coefficient K_e in the parameterisation formulas for the synoptic-eddy heat and moisture fluxes applied in the model (see Fig. 3a, b and the accompanying text below). We note that, unlike all the other presented EMICs, the EcBilt-CLIO model explicitly resolves the weather patterns (see Table 2) and does not employ, in particular, the parameterisation schemes for the description of the synoptic-scale ensemble momentum, heat and moisture fluxes.

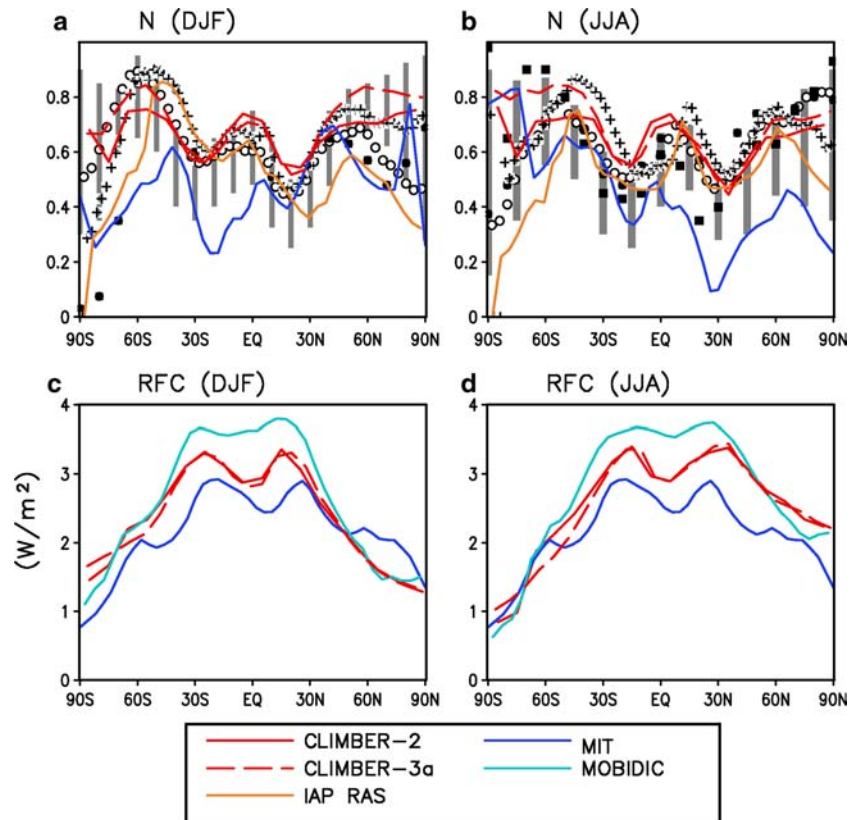
For now, there exist no generally accepted unified conceptual theories treating the ensembles of the transient synoptic-scale eddies/waves and the ageostrophic (e.g. the mean meridional circulation, the monsoon circulation, etc.) patterns of the large-scale long-term atmospheric motion. This problem is of crucial importance, specifically in modelling climates somewhat far from the present-day conditions. With regard to the used in the majority of EMICs ensemble method for the description of the synoptic eddies/waves, a nontrivial problem is the elucidation of the range of accuracy with which the synoptic eddy/wave ensembles can be represented in terms of the “macrodiffusion” process. This latter assumption forms the basis for parameterisations of the synoptic component in most EMICs. [We note here that one of the first parameterisations for the synoptic eddy/wave transport of heat and momentum in terms of the climate variables, similar to those used in most EMICs described in this study, was proposed

in Saltzman and Vernekar (1968, 1971, 1972).] The encouraging circumstance, however, is that the corresponding formulas, e.g. in the CLIMBER-2, CLIMBER-3 α , EcBilt-CLIO, IAP RAS, MIT and MoBidiC models, are not empirical curve fitting formulas but the intrinsic attributes of the background concepts and theories which are applied for the description of the dominant mechanisms of the generation, nonlinear evolution and decay of the individual synoptic eddies/waves and their ensemble characteristics. A fast turnaround time of EMICs provides a possibility to perform a large number of the test runs replacing different modules, mechanisms and feedbacks by the alternative ones (as is done, e.g. in the CLIMBER-3 α and the UVic models), which can help considerably in the study of the aforementioned fundamental problems.

2.5 Evaporation/transpiration

The intercomparison of the simulations of evaporation and transpiration (E) by the EMICs could be instructive for the highlighting of the salient features of the hydrological cycle in the individual models. Figure 2c, d portrays the latitudinal distribution of the zonally averaged E in the EMICs for DJF (panel c) and JJA (panel d) as compared with the empirical (i.e., indirect, based on the empirical formulas and/or reanalysis) data. As seen in the figure, all the EMIC results satisfactorily fit the empirical data in the middle and high latitudes of the NH and SH in DJF (panel c).

Fig. 4 Latitudinal distribution of the zonally averaged total cloud amount N (as a fraction of unity) in CLIMBER-2, CLIMBER-3 α , IAP RAS and MIT (a, b) and the direct radiative forcing due to CO₂ at the top of the atmosphere (as defined in the text) in the CLIMBER-2, CLIMBER-3 α , MIT and MoBidiC models (c, d) for DJF (a, c) and JJA (b, d). For the comparison, in a and b the relevant observational data on N are displayed from Berlyand and Strokina (1980) (open circles), Rossow et al. (1991) (closed circles), Rossow and Schiffer (1999) (crosses) and Stowe et al. (2002) (right panel, closed squares). The vertical bars in panels a and b denote the range of GCM results in the simulations of N in the AMIP GCMs as derived from the results presented in IPCC (1995) and Gates et al. (1999). [See legend to the figure for EMIC identification.]



In the tropics, the spread in the EMIC results on E is larger for DJF. For example, the MPM curve lies somewhat below the empirical curves, whereas the IAP RAS and MIT models overestimate E , respectively, in the SH and NH. CLIMBER-2 produces somewhat “flat” latitudinal distribution of the evaporation in the tropics for both seasons.

The low values of the evaporation in the SH tropical atmosphere in the MPM model are apparently due to the prescribed constant value of the Dalton number in the “bulk” formula describing E in the model. Actually, this number is a function of the surface roughness, as well as the height and the characteristics of the stability of the atmospheric surface layer which are conventionally expressed in terms of the “bulk” Richardson number for this layer.

In essence, the Dalton number strongly increases with the convective conditions which are inherent in the tropical atmosphere, especially in the vicinity of the so-called thermal equator, which has a rather pronounced seasonal cycle in its location that follows, to a first approximation, the seasonal shift in the ITCZ (Intertropical Convergence Zone) position. In the “bulk” formula for E the above-mentioned increase in the Dalton number just compensates, to some extent, the minimum in the surface winds in the vicinity of the thermal equator, as well as in the tropical atmosphere of the summer hemisphere. In these regions, the surface winds are relatively weak (approximately half as large) but the surface temperatures and convective

activity are higher, in comparison, respectively, to those at the analogous latitudes of the tropical atmosphere in the winter hemisphere. This results in a quasi-bimodal shape of the latitudinal distribution of the zonally averaged E in the tropics (with more pronounced maximum in the winter hemisphere). As is seen from Fig. 2c, d, CLIMBER-2, CLIMBER-3 α and IAP RAS generally capture the above-mentioned quasi-bimodal structure of the zonally averaged E in the tropics.

2.6 P-E

The zonally averaged precipitation minus evaporation ($P-E$) in the EMICs are displayed in Fig. 2e, f, together with the corresponding empirical data for this quantity. This figure reveals the problem of modelling the values of a quantity which is calculated in the majority of EMICs (except for MoBidiC) as a second-order difference between the two first-order fields of precipitation and evaporation. [In MoBidiC, $P-E$ is calculated as the divergence of the horizontal moisture flux due to the eddies and the mean meridional circulation.] Nevertheless, the EMIC results are in reasonable agreement with the above-mentioned empirical estimations from Peixoto and Oort (1983), if one takes into account the discrepancy between the results of GCM simulation of $P-E$ and their deviation from the relevant observed values reported in Gates et al. (1999) in relation to the AMIP GCM simulations of $P-E$ over the ocean for DJF. It is

worth noting, however, that the scatter of the corresponding curves makes it somewhat problematic to provide an accurate description of the $P-E$ latitudinal distribution in both of GCMs and EMICs, which could be critical for the accurate simulation of the global ocean thermohaline circulation.

2.7 Latent heat fluxes and cloudiness

Five EMICs participating in the intercomparison study (CLIMBER-2, CLIMBER-3 α , IAP RAS, MIT and MoBidiC), with the detailed atmospheric modules, presented their results on modelling (1) the zonally averaged latent heat fluxes (CLIMBER-2, CLIMBER-3 α , MIT and MoBidiC) as attributed to the synoptic eddies (F_{le}) and the atmospheric mean meridional circulation (F_{lm}), as well as (2) the total cloud amounts N (CLIMBER-2, CLIMBER-3 α , IAP RAS and MIT).

Figure 3a, b shows the latitudinal distribution of F_{le} in CLIMBER-2, CLIMBER-3 α , MIT and MoBidiC. As can be seen from Fig. 3a, b, all EMICs simulate the latitudinal distribution of F_{le} rather well in the SH for DJF (panel a) and JJA (panel b). In the NH, the deviation of the EMIC results from the empirical data for summer is more pronounced, due to the somewhat overestimated amplitude of the seasonal cycle of F_{le} . This could be due to the problem of an adequate description of the seasonal cycle of F_{le} in terms of the coefficient of the “macroturbulent diffusion” for the water vapour K_e as a function of the static stability parameter and the horizontal temperature gradient. In this way, the somewhat high dependence of F_{le} on the above-mentioned temperature gradient is seen in each of the EMICs. Note that in CLIMBER-2 and CLIMBER-3 α a simplified version of the nonstationary advection-diffusion-type partial differential equations (PDEs) developed in Petoukhov et al. (1998, 2003) for the synoptic second moments is implemented. This simplified version of the aforementioned PDEs just results in the diffusion-type formulas for the heat and moisture fluxes due to the ensembles of the transient atmospheric eddies/waves, in terms of the coefficients of the “macroturbulent diffusion”. In the MoBidiC model, K_e is assigned from the present-day-climate observational data on the zonally averaged meridional flux of the quasi-geostrophic potential vorticity (QGPV) due to eddies and the meridional gradient of the zonally averaged QGPV, except for the tropics, where K_e is assumed to be proportional to the fourth power of the present-day-climate meridional gradient of the zonally averaged surface air temperature.

Figure 3c, d is analogous to Fig. 3a, b but for the latitudinal distribution of the vertically and longitudinally integrated northward flux of latent heat F_{lm} due to the mean meridional circulation. The overall structure of the flux is captured in the CLIMBER-2, CLIMBER-3 α and MIT models fairly well, although the MIT model slightly overestimates the maxima of F_{lm} in the tropics

associated with the Hadley cells, while CLIMBER-2 and CLIMBER-3 α somewhat underestimate (overestimate) this flux in the NH Hadley cell for DJF (JJA), most likely for the reasons mentioned in the previous paragraph. Specifically, the contribution from the cumuli convection to the static stability parameter deserves further consideration. In MoBidiC, the mean meridional circulation is represented by the Hadley cells only. These seem to be too broad in the model, which results in a too broad meridional structure of F_{lm} .

Figure 4a, b illustrates the performance of the CLIMBER-2, CLIMBER-3 α , IAP RAS and MIT models in modelling the zonally averaged total cloud amount N for DJF (panel a) and JJA (panel b) in comparison with the observationally based data. As seen in the both panels, there exists a rather large discrepancy between the sets of the observational data, especially in the high latitudes of the NH and over Antarctica. On the other hand, the subtropical minima and the equatorial and the SH mid-latitude maxima are captured in the data and the EMIC simulations.

At the same time, the absolute values of N in the EMICs differ substantially in middle and high latitudes of the NH for JJA. By and large, the values of N are higher in CLIMBER-2, CLIMBER-3 α and IAP RAS in the above-mentioned latitudes and season, as compared with those in the MIT model. Presumably, this is due to a somewhat low magnitude of the synoptic-scale activity and the rather faint intensity of the mid- and high-latitude branches of the mean meridional circulation for the NH summer in the MIT model. The latter may be caused by the rather low magnitudes (resulting from a somewhat overestimated swing of the seasonal variations) of the meridional latent heat fluxes due to the large-scale eddies and the mean meridional circulation for the NH summer in the MIT model (see Fig. 3a–d).

As is seen from Fig. 4a, b, the CLIMBER-2 and MIT models have a negative “kink-like” peculiarity in the latitudinal distribution of N in the high latitudes of the SH in the transition zone from the open ocean to the packed sea ice and the Antarctic ice sheet. This feature is not seen in the observational curves (except for that from Stowe et al. (2002)) and deserves further consideration. Also, the MIT model shows the marked broad positive “kink-like” feature in the latitudinal distribution of N in the NH for DJF in the transition zone from the land to the packed polar sea ice via the open ocean. This is probably due to the somewhat broad “strip” of the open ocean in the winter Arctic in the model which could result from the slightly low sensitivity of the sea ice area in the MIT model to the summer-to-winter change in thermal regime (see Table 7). We will touch upon this problem below when discussing the equilibrium and transient 2 \times CO $_2$ runs. As a whole, Fig. 4a, b demonstrates that the quality of the simulation of the zonally averaged total cloud amount in the EMICs is close to that of the AMIP GCMs. Nonetheless, the IAP RAS and MIT results are, at some latitudes, outside the range of GCM results. In the IAP RAS model, low values of N

in the polar regions are presumably the result of a too simplified description of the cryosphere (in particular, sea ice and Antarctic ice sheet) processes in the model. We also note, however, the noticeable discrepancy among the observational data depicted in Fig. 4a, b.

2.8 CO₂ direct radiative forcing

Intercomparison of the longwave radiative schemes in EMICs is illustrated by Fig. 4c, d, where the direct radiative forcing due to CO₂ at the top of the atmosphere (RFC) is shown for CLIMBER-2, CLIMBER-3 α , MIT and MoBidiC for DJF (panel c) and JJA (panel d).

In this paper, RFC is defined as the difference between the outgoing longwave radiation in the model computed at 280 ppm and 560 ppm CO₂, with fixed (corresponding to 280 ppm CO₂) values of all the other model parameters and variables. Generally speaking, the comparison of the results depicted in Fig. 4c, d can by no means be regarded as a straightforward way of comparing of the radiative schemes used in the models. Nevertheless, it provides some insight into the degree of consistency between the models. From Fig. 4c, d, we observe that the RFC is qualitatively similar in each of the EMICs.

By and large, the discrepancy between the EMIC curves in Fig. 4c, d is smaller in the high latitudes of the winter hemisphere where the atmospheric water vapour content is a minimum and at those latitudes where the total cloud amount converges in the models (cf. Fig. 4a, b, where, in particular, the total cloud amount N in CLIMBER-2, CLIMBER-3 α and MIT is depicted). The above-mentioned discrepancy is the highest in the middle latitudes of the summer hemisphere and in the tropics. Just in these latitudinal ranges the divergence of N curves for the CLIMBER-2 (and CLIMBER-3 α) and MIT models is largest (cf. Fig. 4a, b). In MoBidiC, the seasonal cloud amount of the effective cloud layer is prescribed based on the Warren et al. (1986, 1988) data on the total cloud cover and cloud type amounts. Note that the calculated (in CLIMBER-2 and CLIMBER-3 α) and prescribed (in MoBidiC, from Ohring and Adler 1978) heights of the effective cloud layer are close to each other but the prescribed N in MoBidiC (not shown in this paper) is higher than that calculated in CLIMBER-2 and CLIMBER-3 α , for the subtropics and tropics. Also, the air temperature and specific humidity at the surface, as well as the vertical distributions of these two characteristics, are close in all four models. All this could indicate that the direct radiative forcing of CO₂ itself, which would take place in the absence of the dissimilarities in the temperature, water vapour and cloud amount distributions in the atmosphere, might be close in the four EMICs shown in Fig. 4c, d. At the same time, a nonlinear interplay between the parameters of the longwave radiative schemes, which depend on CO₂ and spatial distributions of temperature, water vapour

and cloudiness, apparently changes from model to model depending on the physics of the applied radiative scheme and the above-mentioned spatial distributions. To a first approximation, the CO₂ direct radiative forcing at the upper boundary of the atmosphere in the four EMICs under consideration is higher for a larger total cloud amount in the model, provided that the other variables entering the longwave radiative schemes are close to each other. This is in qualitative agreement with the theory of the radiative transfer in the atmosphere, for realistic vertical distributions of the atmospheric temperature, water vapor, cloudiness and CO₂ (see, e.g. Goody 1964). Clearly, the above comments point to the need for a detailed intercomparison of the EMIC radiative schemes in the future.

It is pertinent to note that the EMIC latitudinal distribution of the CO₂ direct radiative forcing at the top of the atmosphere as shown in Fig. 4c, d is in concert with that at the tropopause in the AGCMs presented in Ramanathan et al. (1979). Also, the range of the above-mentioned forcing in the EMICs is very close to the range for the AGCMs (about 1W/m²) reported in Cess et al. (1993). We would like to emphasise that the higher CO₂ direct radiative forcing in a model does not necessarily invoke a higher response of the model climate variables (e.g. the global surface air temperature and precipitation) to the change in the CO₂ content. This response strongly depends on the feedbacks between the model climate variables and the applied parameterisations for one or more climate characteristics (e.g. cloudiness).

2.9 The Atlantic overturning circulation

The Atlantic overturning thermohaline circulation (AOTHC) is one of the essential features of the global ocean circulation. The AOTHC is a highly sensitive component of the climate system and may exhibit more than one distinct mode of operation. For example, there exists geological evidence that during some episodes in the Tertiary, the North Atlantic deep water was formed at relatively low latitudes rather than in high latitudes, as in today's ocean. A proper physical description of the above thermohaline circulation modes, as well as determining the mechanisms for the switch from one mode to another are challenges not only for paleoclimate investigators but also for the exploration into the problem of the current climate stability under different (e.g. anthropogenic) forcing and future climate projections. For these reasons, the reproduction of a realistic spatial structure and intensity of the present AOTHC, as well as the attributed heat and freshwater fluxes, is one of the necessary elements of any modern climate model. Further, the stability of the oceanic modes in a climate model may drastically depend on the special structural features of the model which determine the position of the climate state "point" in a phase diagram (and the shape of the diagram itself) in the relevant phase space.

In this paper, we restrict our attention to three important characteristics of the AOTHC: the maximum value of the North Atlantic overturning streamfunction (MAOSF) below the Ekman layer, the value of the North Atlantic heat flux at the latitude of its maximum, and the South Atlantic freshwater flux at 30°S.

Table 5 lists the maximum value of the North Atlantic overturning streamfunction as derived from observationally based estimations and from AOGCMs for the present-day climate conditions, and seven EMICs for the analysed “Equilibrium 1×CO₂” run 1 (the IAP RAS model is missing in Table 5). As is seen from Table 5, the results of the EMICs fall into the range of GCM results, and the maximum value of the North Atlantic overturning streamfunction in the majority of the models—both GCMs and EMICs—is higher as compared with the cited observationally based

estimates (except for Talley et al. 2003). In this context, it is worth mentioning that the relatively low value of the MAOSF in CLIMBER-3 α is basically due to the low value of vertical diffusivity k_{od} employed (a background value of only 0.1 cm² s⁻¹). With the background value of k_{od} of 0.4 cm² s⁻¹, the MAOSF equals 15 Sv in the CLIMBER-3 α model (Montoya et al. 2004).

Most of the oceanic heat transport in the North Atlantic is thought to be associated with the AOTHC. In view of this, the North Atlantic heat transport is an important indicator of the role the AOTHC plays in the ocean energy cycle, in various climate models. Moreover, the North Atlantic heat transport is one of the characteristics which can itself regulate the intensity of the AOTHC, which is one of the most important branches of the world ocean conveyor. The magnitude of the above-mentioned oceanic characteristics in EMICs, for

Fig. 5 The equilibrium change of the zonally averaged SAT (in °C) (a, b), planetary albedo (as a fraction of unity) (c, d) and outgoing longwave radiation (in W/m²) (e, f) in EMICs due to CO₂ doubling, for DJF (a, c, e) and JJA (b, d, f). The vertical bars in a, b represent the range of GCM results for the equilibrium mean annual change of zonally averaged SAT in the GCMs which took part in the equilibrium CO₂ doubling intercomparison project (Le Treut and McAvaney 2000). [See legend to figure for model identification. IAP RAS missing for OLR in e, f]

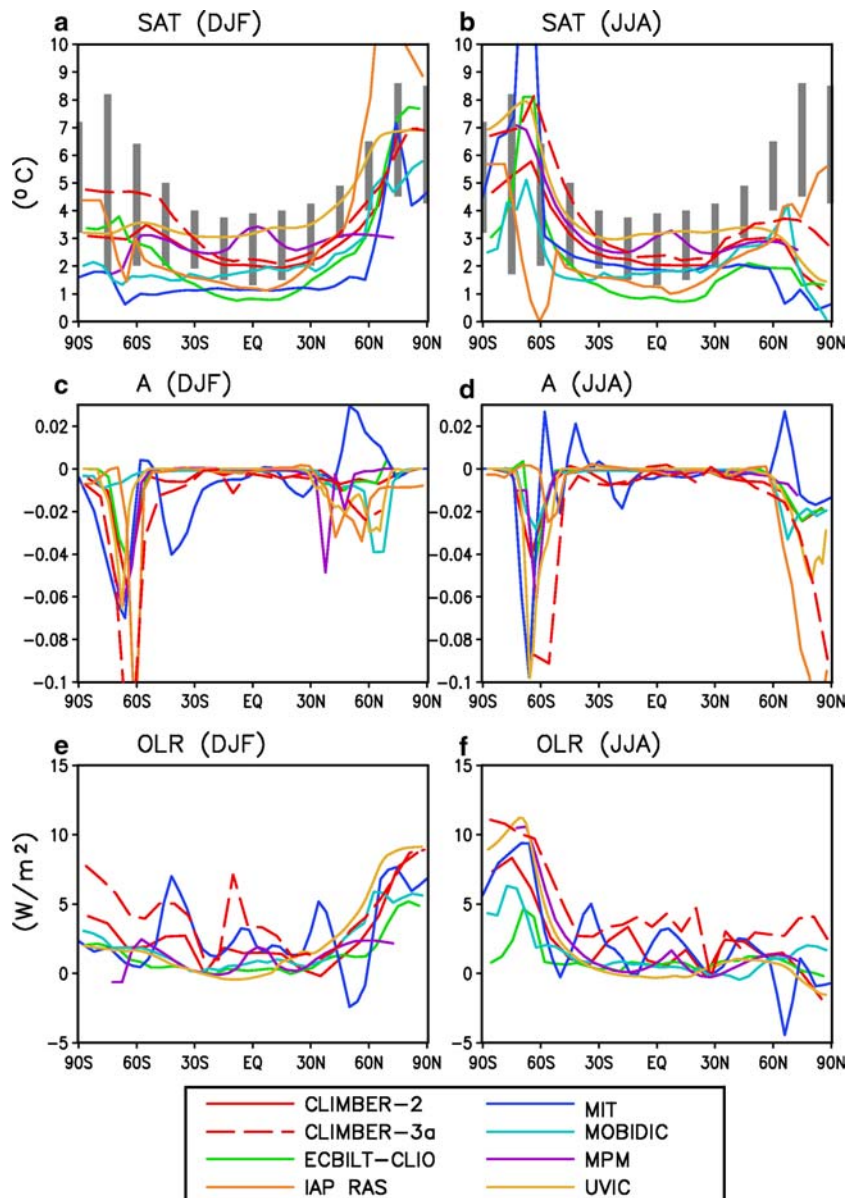
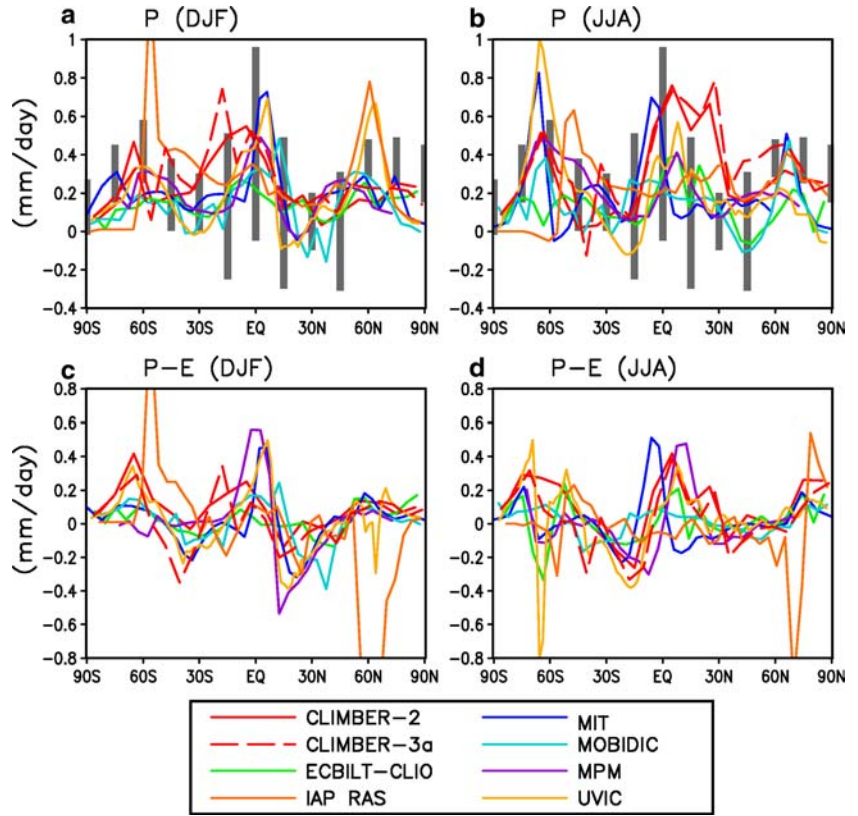


Fig. 6 The same as in Fig. 5 but for the equilibrium change of zonally averaged precipitation (in mm/day) (a, b) and precipitation minus evaporation (in mm/day) (c, d) in the EMICs due to CO₂ doubling, for DJF (a,c) and JJA (b,d). The vertical bars in a, b show the range of GCM results in the performed in the framework of the equilibrium CO₂ doubling intercomparison project (Le Treut and McAvaney 2000) simulations of the change in the mean annual precipitation. [See legend to figure for model identification.]



the present-day conditions, is illustrated by Table 6, where the mean annual value F_{hm} of the North Atlantic heat flux is given at the latitude ϕ_{hm} of its maximum.

[The IAP RAS model is missing in the F_{hm} and ϕ_{hm} entries of Table 6.] For all EMICs, F_{hm} falls into the 0.7 PW to 1.1 PW range, and ϕ_{hm} ranges from 16°N to 25°N, which is within the uncertainty of the range of the empirical estimates for these two quantities reported in Hastenrath (1982), Talley (1984), Hsiung (1985), and Trenberth and Solomon (1994). As is the case with the MAOSF, the value of F_{hm} in Table 6 for CLIMBER-3 α corresponds to the background value of the vertical diffusivity of 0.1 cm² s⁻¹, and F_{hm} increases with the increase in the value of k_{od} in the model (Montoya et al. 2004).

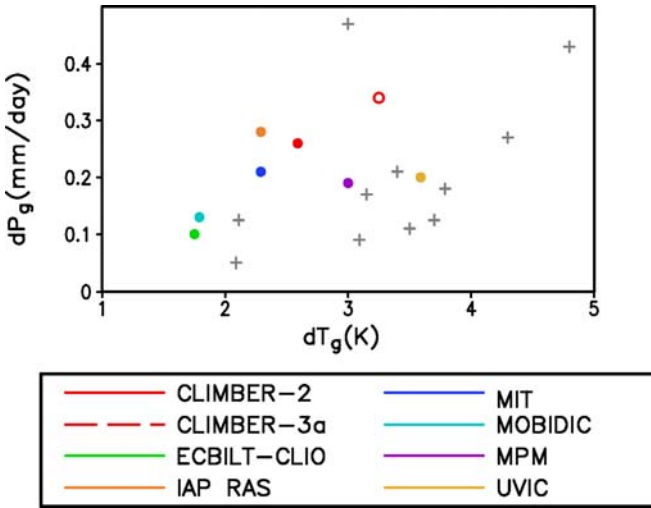


Fig. 7 A scatter plot of the equilibrium changes in the mean annual global surface air temperature (dT_g , x axis, in °C) and precipitation (dP_g , y axis, in mm/day) in the EMICs combined with the analogous results (crosses) produced by GCMs which took part in the equilibrium CO₂ doubling intercomparison project reported in Le Treut and McAvaney (2000). [See legend to figure for model identification; the CLIMBER-2 and CLIMBER-3 α results are shown by closed and open red circles, respectively.]

The EMIC results on the simulation of the oceanic freshwater flux due to the thermohaline circulation in the South Atlantic differ much more widely, as seen in the fourth column of Table 6, where the values of the Atlantic freshwater flux F_{fw} at 30°S are presented. The existence of these large differences in F_{fw} could be of crucial importance for determining the stability of the AOTHC in climate models (Rahmstorf 1996). The uncertainty in the corresponding empirical data on F_{fw} is also high [in Baumgartner and Reichel (1975), Dobrolyubov (1991), Holfort (1994) and Schiller (1995) F_{fw} ranges from -0.05 Sv to 0.58 Sv].

All the EMICs presented in this paper cannot describe El Niño-Southern Oscillation (ENSO) dynamics, mainly because of their low horizontal resolution, as compared to those models that have an explicit description of ENSO. Because of its importance, this latter phenomenon should be parameterised in future

modifications of EMICs, leaning upon the ideas implemented, e.g. in the Cane-Zebiak (Zebiak and Cane 1987) model. Also, it is worth noting that the CLIMBER-2, MoBidiC and MPM models do not resolve the macro-scale oceanic gyres because of the employment of the zonally averaged ocean modules (see Tables 1, 3). These three EMICs could be improved by including a parameterisation for the oceanic gyre heat fluxes, like that proposed in Mann (1998).

2.10 Sea ice area

Modelling a realistic sea ice cover is an important and difficult problem for coupled climate models because of the strong sea ice albedo feedback and the complicated sea ice rheology, which influences its development and dynamics. Table 7 shows the results of the simulation of the Northern (NHI) and Southern (SHI) Hemisphere sea ice areas for DJF and JJA in the EMICs and also the observationally based data on the present-day sea ice cover from Robock (1980) and Ropelewski (1989) (the IAP RAS model is missing in Table 7; note, there is no Arctic Ocean in the MPM model, see Table 3). Despite a simplified description of the sea ice dynamics in the majority of EMICs (except for the CLIMBER-3 α , EcBilt-CLIO and UVic models, see Tables 2 and 4 and Introduction), the EMIC results may be thought of as being satisfactory, for most models. In Table 7, the maximum (NHI_{max}, SHI_{max}) and minimum (NHI_{min}, SHI_{min}) sea ice areas in the NH and the SH are also shown for the observationally based estimates and for the EMICs. In EcBilt-CLIO, NHI_{max}, SHI_{max} and NHI_{min}, SHI_{min} agree nicely with the observations, while in CLIMBER-3 α NHI_{min} is too low. The MoBidiC model, underestimates the minimum sea ice areas in both hemispheres, which could be attributed, in particular, to a quasi-zonal structure and coarse latitudinal resolution of the 3-basin ocean module with a zonally averaged atmosphere above. The MIT model also underestimates sea ice extent, especially in the NH, which could be a result of a too simplified geometry of the ocean module. The sea ice area in the CLIMBER-3 α model is overestimated for the SH. Presumably, this is due to somewhat low temperatures of the high-latitude Southern Ocean and a rather sluggish Antarctic Circumpolar Current in the model.

3 “Equilibrium” response to a doubled pre-industrial CO₂ content

In Sect. 2, the results of the “Equilibrium 1 \times CO₂” run 1 under constant pre-industrial (280 ppm) atmospheric CO₂ concentration in the analysed eight EMICs were described. In Sects. 3, and 4, the descriptions of the results are given of modelling the transient and equilibrium responses of the same eight EMICs to CO₂

doubling in the atmosphere. The participating groups conducted the following runs 2 and 3:

“Transient 2 \times CO₂” run 2, with an increase in atmospheric CO₂ concentration of 1 per cent per year compounded, beginning with the “equilibrium” pre-industrial CO₂ state obtained at the end of the described in Sect. 2 “Equilibrium 1 \times CO₂” run 1, until a doubled CO₂ is reached.

“Equilibrium 2 \times CO₂” run 3: Continuation of the run 2 under constant (doubled) atmosphere CO₂ concentration until “equilibrium” was reached. (The total duration of runs 2 and 3 was more than 1,500 years.)

The results obtained at the end of the “Equilibrium 2 \times CO₂” run 3 is our initial interest. We thus are first focussing on the “equilibrium” response of the Earth’s climate system in the EMICs to CO₂ doubling in the atmosphere, which is described in this section.

Figure 5a, b shows the “equilibrium” change of the zonally averaged surface air temperature SAT (denoted by ΔT in the text below) in the EMICs due to CO₂ doubling, for DJF (panel a) and JJA (panel b), along with the range of GCM results (as defined above in the Introduction) which were obtained in the equilibrium CO₂ doubling intercomparison project (Le Treut and McAvaney 2000). Eleven AOGCMs with a slab ocean as the oceanic module took part in this latter project. [From here on the term “equilibrium” change/response signifies the difference between the values of any climate characteristics averaged over the last 10 years of the above-mentioned “Equilibrium 2 \times CO₂” run 3 and “Equilibrium 1 \times CO₂” run 1. We note also that in Le Treut and McAvaney (2000) the results corresponding to the mean annual conditions only are shown.] The majority of the EMICs demonstrate the same qualitative pattern of temperature change, which is characterised by a large increase in SAT (presumably associated with snow/ice surface albedo and cloud and lapse rate feedbacks) at high latitudes of the winter hemisphere and a relatively smaller change in the tropics and subtropics of the summer hemisphere. However, the amplitude of the above-mentioned pattern differs widely from one model to another. As can be seen from Fig. 5a, b, the dispersion of the values of ΔT in the EMICs and GCMs is of the same order in the tropics and subtropics of the Northern Hemisphere (NH) and the Southern Hemisphere (SH). At the same time, in the subpolar and polar regions, EMICs demonstrate a rather large scatter in the results (e.g. IAP RAS (MIT) significantly underestimates (overestimates) the increase in SAT in the (60–70) $^{\circ}$ S latitudinal belt over the polar Southern Ocean in JJA, as compared with the results of the other EMICs, while IAP RAS shows the higher sensitivity of the NH polar temperatures, both in DJF and JJA).

It is likely that some of these features in the latitudinal distribution of ΔT correlate with the different efficiency of cloud and surface albedo feedbacks in the EMICs. As an example, the above-mentioned “cold kink” in the (60–70) $^{\circ}$ S latitudinal range for JJA in the IAP RAS model is likely due to an increase in the

convective cloud amount (not shown in this paper) caused by the intensification of the convective activity over the warmer open ocean in the subantarctic SH latitudes in the model. The above-mentioned increase in the convective cloud amount and the accompanying decrease in the downward solar flux at the surface nearly compensate, in the IAP RAS model, the decrease—due to warming—in the sea ice/open ocean surface albedo in the considered latitudinal range. This results in a low response of SAT (and planetary albedo, see Fig. 5d) to a CO₂ doubling in the model. The above noted “warm” kink in the response of SAT to a CO₂ doubling in the MIT model for JJA in the (60–70)°S latitudinal belt is likely to be associated with the decrease in the planetary albedo over the polar Southern Ocean (see Fig. 5d) in the model. This, in turn, is caused by a rather pronounced decrease in the sea ice concentration (see Fig. 10f below)—and hence surface albedo—in the polar Southern Ocean in the MIT model, although the change in the total cloud amount (not shown in this paper) is positive in the MIT model, as it is in IAP RAS, for the same season and latitudinal range. This poses a problem of comparing the relative strength of the mentioned climate feedbacks (see the Introduction) in different EMICs. By and large, in most EMICs the average change over the DJF and JJA seasons of the zonal SAT due to CO₂ doubling is only weakly asymmetric about the equator.

Figure 5c, d illustrates the latitudinal structure of the equilibrium change in zonally averaged planetary albedo (designated by ΔA in the text below) in EMICs caused by CO₂ doubling. As can be seen from Fig. 5c, d, all the models are qualitatively consistent with each other in the tropical regions of the NH and SH, for both boreal winter (panel c) and summer (panel d) averages. At the same time, the dispersion of the EMIC responses to the change in CO₂ content is wide for the middle and high latitudes of the NH and SH (specifically, in the regions where snow- and ice-covered areas give way to snow- and ice-free ones). As in the case for ΔT , the EMICs reveal noticeable scatter in the values of ΔA at some latitudes. In particular, the MIT model shows the marked latitudinal variations in the change of the planetary albedo which are apparently closely correlated to the above-mentioned equilibrium changes in the total cloud amount N and sea ice area due to CO₂ doubling for the corresponding latitudinal ranges and seasons in the model.

Except for the CLIMBER-2, CLIMBER-3 α , IAP RAS and MIT models (in which cloudiness and the atmospheric mean meridional circulation are not prescribed or implicitly accounted for parameters but are model variables) and MoBidiC (in this model the seasonal cloudiness is specified and the mean meridional circulation is one of the modelled climatic fields), the latitudinal structure of the equilibrium change in the zonally averaged outgoing longwave radiation (OLR) due to doubling of CO₂ content in the atmosphere is rather smooth and consistent in the other EMICs (see Fig. 5e, f), for both DJF (panel e) and JJA (panel f)

seasons. [IAP RAS is missing in Fig. 5e, f.] Generally speaking, the detailed geographical variation of the equilibrium change in OLR is more pronounced in models with the more elaborated scheme of cloudiness and dynamics or with the explicitly prescribed seasonal cloudiness and dynamics; the patterns of the equilibrium change in OLR are far smoother in EMICs with simple or no module of cloudiness. This conclusion is supported by the GCM results: e.g. Fig. 7 from Le Treut and McAvaney (2000) illustrates a highly inhomogeneous latitudinal distribution of the equilibrium response of OLR to CO₂ doubling in the HADCM, BMRC, MPI, NCAR and GISS models, which is similar to the CLIMBER-2, MIT and MoBidiC dispersion in the latitudinal distribution of this quantity. In all the EMICs shown in Fig. 5e, f, the equilibrium change in OLR is marked by an absolute maximum in the polar latitudes of the winter hemisphere and has less pronounced variations in the tropics and summer hemisphere. This feature is by and large consistent with the change in SAT due to the snow/sea ice surface albedo feedback in the polar regions (cf. Figs. 5a, b, e, f).

Less agreement is found between the results for different EMICs in modelling the equilibrium change of zonally averaged precipitation (hereafter referred to as ΔP) to CO₂ doubling (Fig. 6a, b). A majority of the models produce an increase in zonally averaged precipitation in the tropics, subpolar and polar regions, for both DJF (panel a) and JJA (panel b). However, the magnitudes and geographical patterns of these increases vary widely from model to model. The simulation of ΔP in the subtropics is less consistent. Figure 6a, b shows that some EMICs display a decrease in zonally averaged precipitation in the subtropics, whereas the others demonstrate an increase in this climate characteristics in the same regions. A comparison of the uncertainty in EMIC results with the range of GCM results from the equilibrium CO₂ doubling intercomparison project (see Fig. 6a, b) indicates that these two uncertainties are of the same order. Specifically, the problem of the sign of ΔP in the subtropics is a challenge for GCMs as well.

Figure 6c, d shows the latitudinal distribution of the equilibrium change of the difference between the zonally averaged precipitation and evaporation in EMICs due to the doubling of the CO₂ content in the atmosphere. As was the case in Fig. 2e, f, this figure reveals the problem of modelling changes in the values of a quantity which is calculated in the majority of EMICs (except for MoBidiC) as a second-order difference between two first-order fields of precipitation and evaporation. [We recall that in MoBidiC, $P-E$ is set equal to the divergence of the horizontal moisture flux due to eddies and the mean meridional circulation]. There is fairly close agreement between most models only for DJF (panel c) in the tropics and middle latitudes; in the subpolar and polar regions for this season, as well as in all the latitudinal belts for JJA (panel d), the divergence of the results is large, with respect to both the magnitude and sign of the equilibrium change in $P-E$.

In Fig. 7, a scatter plot is displayed of the equilibrium changes in the mean annual global surface air temperature $d T_g$ (x axis) and precipitation $d P_g$ (y axis) in the EMICs. As is evident from the picture, the results of the EMICs by and large fall into the range of GCM results from the equilibrium CO₂ doubling intercomparison project (Le Treut and McAvaney 2000). In this context, it is worth noting that the relatively low values of $d T_g$ and $d P_g$ in the EcBilt-CLIO model presumably resulted from their run not reaching the equilibration with a doubled CO₂ content in the atmosphere (the duration of the EcBilt-CLIO “Equilibrium 2×CO₂” run 3 was about 1,000 years, see Figs. 9b and 10b below). Furthermore, as was already noted, the results of the “equilibrium” 2×CO₂ GCM runs shown in Fig. 7 are obtained in the model versions with a slab ocean as the oceanic module (Le Treut and McAvaney 2000), so that the equilibration time in those models was relatively short. At the same time, all EMICs participating in the intercomparison include a deep ocean module and most EMICs do not reach a “final” equilibrium state with a doubled CO₂, even after the 1500 year run (see Figs. 9b, 10b below). However, a “final” equilibrium state in all EMICs is only slightly more warm and rainy than that shown in Fig. 7. But we note that the CLIMBER-3α model data are on the upper extreme regarding the precipitation change dP_g , for the EMICs and for most of the GCMs.

4 “Transient” and combined “Transient” and “Equilibrium” 2×CO₂ runs.

In this section, the results of the “Transient 2×CO₂” run 2 (with an increase in atmosphere CO₂ concentration by 1 per cent per year until doubling is reached) are first presented. Then the combined results are described for the “Transient 2×CO₂” run 2 and “Equilibrium 2×CO₂” run 3—the continuation of the run 2 under constant (doubled) atmosphere CO₂ content until “equilibrium”.

Figures 8a, b display the change in SAT for the “Transient 2×CO₂” run 2 in the EMICs for DJF (panel a) and JJA (panel b), respectively. The time averaging over the years 66 through 75 used in these figures is representative of the so-called transient climate response to CO₂ doubling, under the given scenario of the rate of the increase in CO₂ concentration (1 per cent per year compounded). It is instructive to compare Figs. 8a, b, respectively, with Figs. 5a, b. These latter figures illustrate the equilibrium change in the same quantity due to CO₂ doubling in the EMICs. The comparison shows that, by and large, the DJF (JJA) transient response has more (less) pronounced asymmetry in the latitudinal distribution, as compared to the equilibrium response. The same conclusion can be inferred from the comparison of the equilibrium changes in the planetary albedo and outgoing longwave radiation (depicted, respectively, in Figs. 5c, d, e, f) with their transient counterparts (the latter are not displayed in this paper). In this context, one of the probable reasons for the asymmetry between the NH and SH mean annual transient responses to an increase in atmospheric greenhouse gas concentrations is given in Goosse and Renssen (2001). They show that the response of the Southern Ocean to an increase in atmospheric greenhouse gas concentrations simulated by EcBilt-CLIO can be decomposed into two different phases. The ocean first dampens the surface warming because of its large heat capacity and then, one century after the major increase in greenhouse gases, the warming is amplified because of a positive feedback that is associated with a stronger oceanic meridional heat transport toward the Southern Ocean. Both effects elicit a much larger long-term decrease in sea ice area in the Southern Ocean than in the Northern Hemisphere in EcBilt-CLIO.

The comparison of Figs. 8a, b, respectively, with Figs. 5a, b reveals that the magnitudes of the transient responses of SAT to CO₂ doubling in the EMICs are on the whole markedly lower than the equilibrium responses (note that different scales are used in the y axis

Fig. 8 Latitudinal distribution of the change, due to atmosphere CO₂ doubling, in the zonally averaged SAT (in °C) for DJF (a) and JJA (b) in the EMICs by the end of the “Transient 2×CO₂” run 2. [See legend to figure for model identification.]

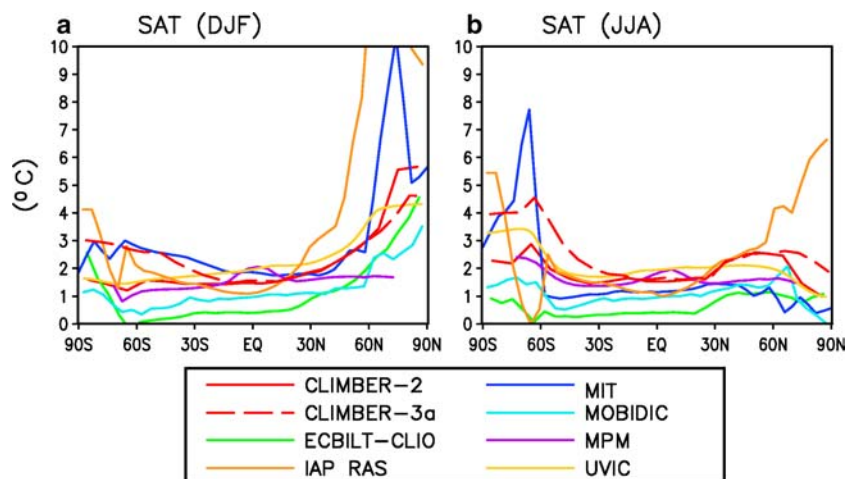
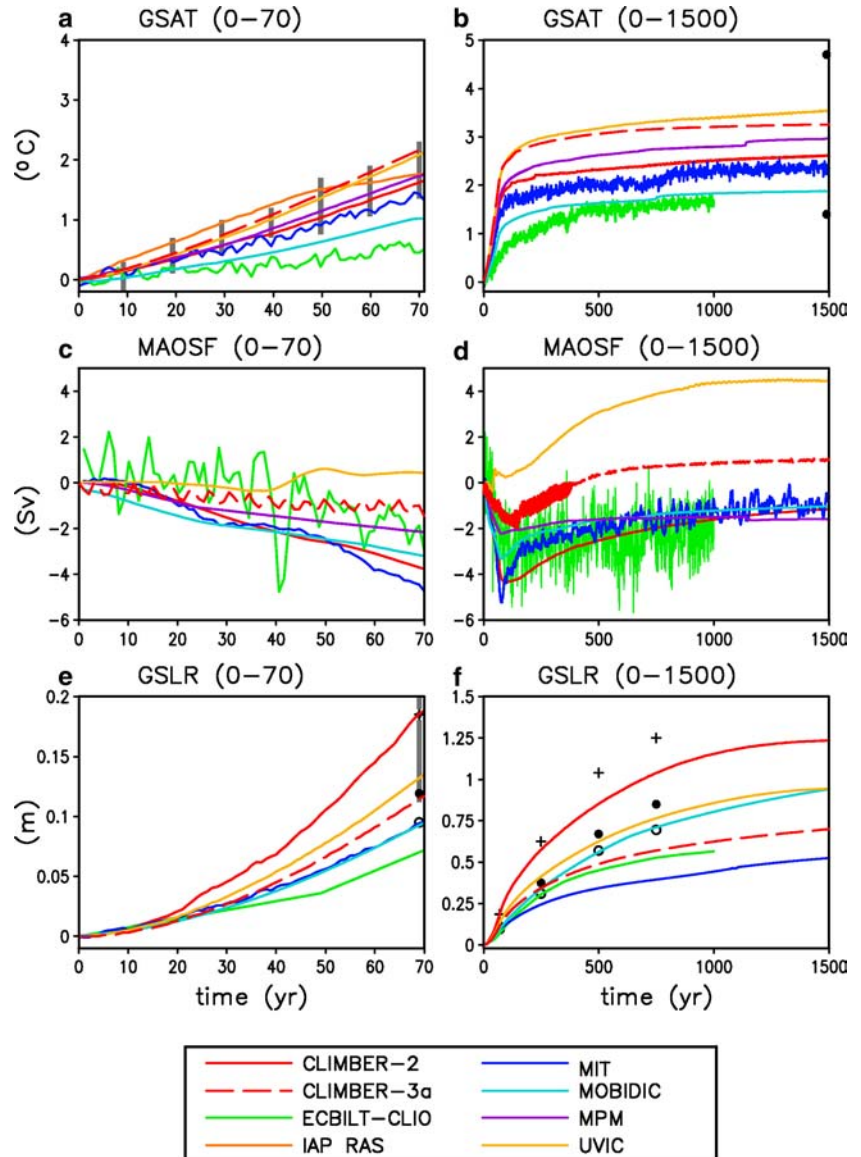


Fig. 9 The time series of the change in the mean annual global SAT (in °C) (a, b) and maximum value of the North Atlantic overturning streamfunction (in Sv) (c, d), and the time series of the global sea level rise due to thermal expansion of sea water (GSLR, in m) (e, f) in the EMICs for the “Transient 2×CO₂” run 2 (a, c, e) and the combined “Transient” and “Equilibrium” 2×CO₂ runs 2 and 3 (b, d, f), beginning with the “equilibrium” pre-industrial CO₂ state obtained in run 1. The vertical bars in a and closed circles in b exhibit, respectively, the scatter in the results of CMIP2 AOGCMs reported in Covey et al. (2003) and the scatter in the results of the equilibrium 2×CO₂ response in CMIP2 AOGCMs displayed in Covey et al. (2000). The vertical bar in e marks the uncertainty in the low and middle projections of the GSLR in the AMIP GCMs reported in IPCC (1995). The crosses, closed circles and open circles in e and f designate, respectively, the presented in IPCC (2001) results from the participating in CMIP2 GFDL, HADCM and ECHAM AOGCMs, for the corresponding scenarios of CO₂ increase [See legend to figure for EMIC identification. IAP RAS is missing in c, d, e, f; MPM missing for GSLR in e, f, see Table 3.]

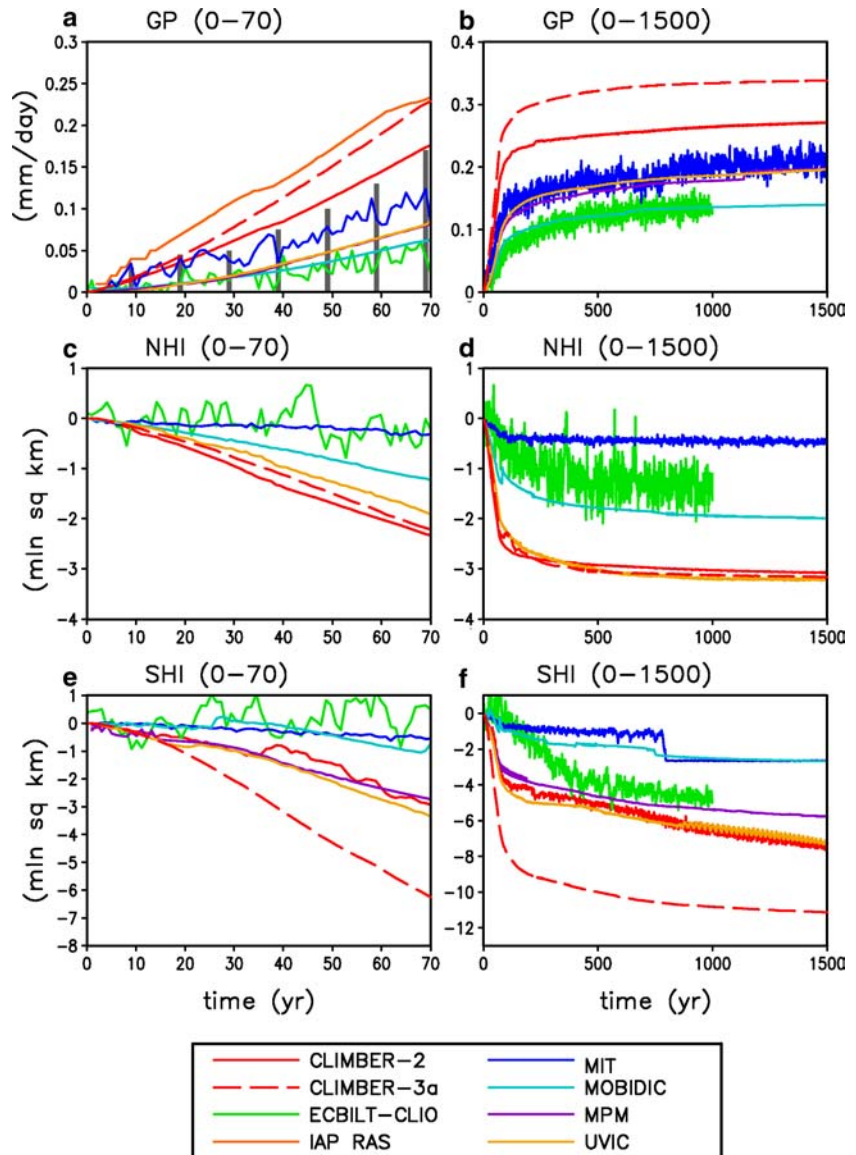


in the respective figures). Similar conclusions are valid for the planetary albedo and outgoing longwave radiation (as well as for P and $P-E$ quantities).

Figure 9a, b shows the time series of the change in the mean annual global surface air temperature (GSAT) in EMICs for the “Transient 2×CO₂” run 2 (panel a) and in the combined “Transient” and “Equilibrium” 2×CO₂ runs 2 and 3 (panel b), beginning with the “equilibrium” pre-industrial CO₂ state obtained in run 1. As mentioned in Le Treut and McAvaney (2000), a broad range is still present in the AOGCM results on modelling the equilibrium response of GSAT to CO₂ doubling in the atmosphere. As can be seen from Fig. 9a, b, for both runs 2 and 3, the EcBilt-CLIO model somewhat underestimates the response of GSAT to the increase in the CO₂ loading of the atmosphere, as compared to all other EMICs. The “equilibrium” climate sensitivity, which we define, for any EMIC, as the difference between the

average over the last 10 years of integration the global surface air temperatures developed in the model by the end of the “Equilibrium” 2×CO₂ run 3 and by the end of the “Equilibrium” 1×CO₂ run 1, is about 1.75°C in the EcBilt-CLIO. Presumably, this relatively low “equilibrium” climate sensitivity is a consequence of a rather low sensitivity in the model of the tropical and subtropical SAT to the atmosphere CO₂ content (see Figs. 5a, b, 8a, b). In general, this feature is inherent in the quasi-geostrophic models, which have a somewhat schematic description of the dynamics and thermodynamics of the tropical atmosphere. We note, however, that EcBilt-CLIO does not reach its “final” equilibration with a doubled CO₂ content in the atmosphere by the end of the 1,000-year “Equilibrium” 2×CO₂ run 3 in the model (see Fig. 9b). The UVic model demonstrates the highest “equilibrium” climate sensitivity (about 3.6°C), among the presented EMICs. The IAP RAS model reveals a

Fig. 10 The same as in Fig. 9 but for the change in the mean annual global precipitation (in mm/day) (a, b), and sea ice area (in 10^6 km²) in the NH (c, d) and SH (e, f). The vertical bars in a indicate the range of GCM results, as derived from the presented in Covey et al. (2003) temporal trends for the same climate characteristics from the CMIP2 AOGCMs. [See legend to figure for model identification. IAP RAS is missing in c, d and e, f; MPM missing for the NH missing for the NH sea ice area in c, d, see Table 3.]



nearly constant response of GSAT (about 2.1°C) to CO₂ doubling in the atmosphere after the first 150 years of integration. For that reason, the IAP RAS curve is not shown in Fig. 9b. By and large both the transient and equilibrium responses of GSAT to the atmosphere CO₂ doubling in the EMICs are within the range of GCM results (as defined above in the Introduction) from the CMIP2 intercomparison project (see Fig. 9a, b) as derived from the results presented by Covey et al. (2000, 2003).

Figure 9c, d displays the time evolution of the change in the maximum value of the North Atlantic overturning streamfunction (MAOSF) for the runs shown in Fig. 9a, b (IAP RAS is missing in Fig. 9c, d, e, f). As seen from Fig. 9c, d, the time series of the change in MAOSF for each EMIC is characterised by a negative “kink” during approximately the first 500 years of the integration, although the amount of the “kink” differs noticeably

from model to model. This behaviour is found in AOGCMs as well. For example, the GFDL AOGCM response to the same scenario of atmosphere CO₂ increase includes changes in the MAOSF which are very similar to that found in CLIMBER-2, except that in the GFDL model the magnitude of a “kink” is roughly twice as large (cf. Fig. 9.25 from IPCC (2001)). It is interesting to note that, in contrast to all the other EMICs, the CLIMBER-3α and the UVic models have a MAOSF at 1,500 year which is larger than the initial value. Also, the variability of the MAOSF drastically decreases in CLIMBER-3α after approximately 350 years of integration, probably due to an abrupt change in the total area of the NH polar convection sites in the model. These are intriguing issues that deserve to be examined in more detail in the future.

Figure 9e, f is the same as Fig. 9c, d but for global sea level rise (GSLR) due to thermal expansion of sea water.

As can be seen from Fig. 9e, f, the EMIC results are close to those of the CMIP2 AOGCMs, although in a number of cases the EMIC values tend to be lower than the AOGCM values. It is instructive to comment on the difference in the simulation of GSLR in CLIMBER-2 and CLIMBER-3 α : the CLIMBER-2 curves in both the left and right panels of Fig. 9e, f lie higher than those for CLIMBER-3 α . This feature is typical of the model results produced when employing an ocean module with isopycnal mixing (as is in CLIMBER-3 α) versus those results for an ocean module with horizontal mixing (as in CLIMBER-2).

Interestingly enough, the global surface air temperature change and the global sea level rise in most EMICs by the end of the “Transient” 2 \times CO₂ run 2 come to only one-third to two-thirds their values in the end of the “Equilibrium” 2 \times CO₂ run 3 (cf. Figs. 9a, b, e, f), which reveals a crucial role the deep ocean plays in the Earth’s climate system response to CO₂ change in the atmosphere (cf. also Figs. 10a, b).

Figure 10a, b is the same as Fig. 9a, b but for time series of the change in the mean annual global precipitation. As can be seen from Fig. 10a, b, all the EMICs (except for the IAP RAS and CLIMBER-3 α models) fall into the range of GCM results from the CMIP2 as can be derived from the results displayed in Covey et al. (2003). After the first 150 years of integration, the IAP RAS model exhibits a nearly constant in time increase in the mean annual global precipitation (about 2.7 mm day⁻¹) in response to CO₂ doubling in the atmosphere. For that reason, the IAP RAS curve is not shown in Fig. 10b.

Figure 10c, d, e, f illustrate the time series for the change in the mean annual sea ice area in the Northern Hemisphere (NHI) and the Southern Hemisphere (SHI) in the EMICs for the same “Transient 2 \times CO₂” run 2 (panels c, e) and combined “Transient” and “Equilibrium” 2 \times CO₂ runs 2 and 3 (panels d, f). MPM is missing data for the change in NHI in Fig. 10c, d (see Table 3), and hence MPM sea ice data are plotted only in Fig. 10e, f. IAP RAS is missing in Fig. 10c, d, e, f. As can be seen from Fig. 10c, d, e, f, the dispersion of the EMIC results in modelling the various sea ice cover characteristics is rather pronounced, and some specific features of the time evolution of the SHI in the EMICs should be clarified (see Fig. 10f). In particular, in the MoBidiC and MIT models a stepwise structure of the time evolution of the sea ice area occurs, which could be a consequence of the implementation in these models of the zonal averaging formalism and rather coarse meridional resolution. Such features can manifest themselves in sudden changes in the ocean mixed layer depth in what is actually a single grid point, which can result in the above-mentioned stepwise structure of the time series of the sea ice area. The CLIMBER-3 α model exhibits a rather high sensitivity of the sea ice area in the SH to CO₂ doubling, which presumably could result from the overestimation of the SHI in this EMIC (see Sect. 2).

5 Conclusions

In summary, the performance of EMICs for the equilibrium 280 ppm CO₂ climate shows:

- a general qualitative and, in many cases, quantitative agreement between the modelled and observed fields of zonally averaged SAT, planetary albedo, outgoing longwave radiation, precipitation, and the North Atlantic overturning thermohaline circulation
- a scatter in the EMIC results that is by and large within the limits of the uncertainty in the results of the present-day climate simulations in AMIP AGCMs and CMIP1 AOGCMs
- a modelled direct radiative forcing due to CO₂ doubling at the top of the atmosphere that is consistent with that in the AGCMs at the tropopause.

At the same time, some gaps are revealed in the EMIC simulations with regard to the details of the latitudinal structure of individual climatic fields. In particular, we note a somewhat overestimated magnitude of the simulated seasonal cycle for the zonally averaged latent heat fluxes due to the synoptic eddies/waves and the mean meridional circulation, and a large dispersion in the modelled magnitudes and positions of peaks and minima in the latitudinal distribution of zonally averaged $P-E$. Modelling of the global hydrological cycle (especially cloudiness), sea ice concentration and oceanic freshwater flux remains the weak point in EMICs, as well as in CMIP1 AOGCMs. Adequate parameterisations have to be developed in the EMICs for the description of some explicitly unresolved energy-related structures, e.g. the macro-scale oceanic gyres (in EMICs with zonal oceanic modules), quasi-stationary planetary-scale thermal and orographic atmospheric waves (in the models with the energy-moisture balance-type atmospheric modules) and ENSO.

The performance of the eight EMICs with respect to the response of the Earth’s climate to an increase in the atmosphere CO₂ concentration reveals:

- a general qualitative agreement (among EMICs) on the overall latitudinal structure of the equilibrium and transient responses of SAT to CO₂ doubling in the atmosphere
- a dispersion of the EMIC results in simulating the equilibrium and transient responses of globally averaged SAT and precipitation to CO₂ doubling which is similar to that in CMIP2 AOGCM results
- a scatter of the EMIC results in the phase space of the equilibrium changes in the global surface temperature and precipitation due to CO₂ doubling, which falls into the range of AGCM (coupled to a slab ocean) results
- a qualitatively close agreement of the EMIC results with those of the CMIP2 AOGCMs in the temporal evolution of the maximum Atlantic overturning streamfunction due to CO₂ doubling

– a qualitatively and quantitatively close agreement of the EMIC results with those of the CMIP2 AOGCMs in the character of the time evolution of the global sea level rise due to CO₂ increase, with higher values of this characteristics in the EMICs with horizontal mixing and lower values in the models with isopycnal mixing in the ocean module

We thus conclude that EMICs could be successfully employed as a useful and highly efficient, in terms of the running time, tool for the assessment of the long-term surface air temperature, precipitation and sea level changes, under a variety of future and past climate scenarios, as well as for testing and validating different concepts and parameterisation schemes for the individual climate mechanisms and feedbacks.

However, a noticeable dispersion is detected in EMIC results as to the latitudinal response to transient and equilibrium CO₂ doubling of some important climate characteristics, e.g. the zonally averaged planetary albedo, outgoing longwave radiation, and *P–E*. A pronounced quantitative discrepancy is revealed in simulating the CO₂-driven changes in the maximum Atlantic overtuning streamfunction and the sea ice areas in the NH and SH. This indicates that the sensitivity of the specific climate processes (e.g. the global hydrological cycle) and feedbacks (e.g. cloud and snow/sea ice surface albedo feedbacks), as well as of their relative strength, to the external (e.g. anthropogenic) forcing might differ widely in EMICs. This necessitates further intercomparison of EMICs, in particular, with respect to the efficiency of climate feedbacks operating in these climate models. A serious problem for the majority of EMICs remains the lack of adequate simulation of interannual and interdecadal climate variability. In this context, the implementation of the nonstationary partial differential equations for treating the atmosphere synoptic-scale eddy/wave ensemble fluxes and variances is of specific interest.

Acknowledgements The contributions of L.A. Mysak and Z. Wang to this paper were supported by the Canadian Natural Sciences and Engineering Research Council and Canadian Foundation for Climate and Atmospheric Sciences. T. Fichet and H. Goosse are research associates with the Belgian National Fund for Scientific Research. A.J. Weaver and M. Eby received funding from the Canadian Natural Sciences and Engineering Research Council and Canadian Foundation for Climate and Atmospheric Sciences. I.I. Mokhov and A.V. Eliseev are supported by the Russian Foundation for Basic Research (grants 05-05-64907, 05-05-65034 and 05-05-65167) and the Russian President Scientific Program (grants 1636.2003.5 and 3570.2004.5). M. Montoya is funded by the Spanish Ministry for Science and Education through the Ramón y Cajal programme. The authors are indebted to the anonymous reviewers for their constructive comments.

References

- Alcamo J, Kreileman GJJ, Leemans R (eds) (1996) Integrated scenarios of global change: results from the IMAGE 2.1 model. *Spec Iss Global Environ Change* 6(4):255–394
- Berlyand TG, Strokina LA (1980) Global distribution of total cloudiness. *Gidrometeoizdat Leningrad*, 71 pp
- Brovkin V, Ganopolski A, Svirezhev Y (1997) A continuous climate-vegetation classification for use in climate-biosphere studies. *Eco Model* 101:251–261
- Campbell GG, Vonder Haar TH (1980) Climatology of radiation budget measurements from satellites. *Atm Sci Paper No 323*, Dept Atmos Sci Colorado State University: 74 pp
- Cess RD, Zhang MH, Potter GL, Barker HW, Colman RA, Dazlich DA, Delegenio AD, Esch M, Fraser JR, Galin V, Gates WL, Hack JJ, Ingram WJ, Kiehl JT, Lacis AA, Letreut H, Li ZX, Liang XZ, Mahfouf JF, McAvaney BJ, Meleshko VP, Morcrette JJ, Randall DA, Roeckner E, Royer JF, Sokolov AP, Sporyshev PV, Taylor KE, Wang WC, Wetherald RT (1993) Uncertainties in carbon dioxide radiative forcing in Atmospheric General Circulation Models. *Science* 262:1252–1255
- Chalikhov DV, Verbitsky MYa (1984) A new Earth climate model. *Nature* 308:609–612
- Claussen M, Mysak LA, Weaver AJ, Crucifix M, Fichet T, Loutre M-F, Weber SL, Alcamo J, Alexeev VA, Berger A, Calov R, Ganopolski A, Goosse H, Lohmann G, Lunkeit F, Mokhov II, Petoukhov V, Stone P, Wang Z (2002) Earth system models of intermediate complexity: closing the gap in the spectrum of climate system models. *Clim Dyn* 18:579–586
- Colman R, Fraser J, Rotstayn L (2001) Climate feedbacks in a general circulation model incorporating prognostic clouds. *Clim Dyn* 17:103–122
- Covey C, Abe-Ouchi A, Boer GJ, Boville BA, Cubasch U, Fairhead L, Flato GM, Gordon H, Guilyardi E, Jiang X, Johns TC, Le Treut H, Madec G, Meehl GA, Miller R, Noda A, Power SB, Roeckner E, Russel G, Schneider EK, Stouffer RJ, Terray L, von Storch J-S (2000) The seasonal cycle in coupled ocean-atmosphere general circulation models. *Clim Dyn* 16:775–787
- Covey C, AchutaRao KM, Cubasch U, Jones P, Lambert SJ, Mann ME, Phillips TJ, Taylor KE (2003) An overview of results from the Coupled Model Intercomparison Project. *Global Planet Change* 37:103–133
- Cox PM (2001) Description of “TRIFFID” Dynamical Global Vegetation Model. Hadley Centre Techn Note HCTN24, Exeter, UK
- Cox PM, Betts RA, Jones CD, Spall SA, Totterdell IJ (2000) Acceleration of global warming due to carbon-cycle feedbacks in a coupled climate model. *Nature* 408:184–187
- Crucifix M, Loutre MF, Tulkens P, Fichet T, Berger A (2002) Climate evolution during the Holocene: a study with an Earth system model of intermediate complexity. *Clim Dyn* 19:43–60
- Demchenko PF, Velichko AA, Eliseev AV, Mokhov II, Nechaev VP (2002) Dependence of permafrost conditions on global warming: comparison of models, scenarios, and paleoclimatic reconstructions. *Izvestiya, Atmos Ocean Phys* 38(2):143–151
- Dickinson RE, Henderson-Sellers A, Kennedy PJ, Wilson MF (1986) Biosphere-Atmosphere Transfer Scheme (BATS) for the NCAR Community Climate Model. NCAR/TN-275+STR, NCAR Boulder, Colorado: 69 pp
- Dickson RR, Brown J (1994) The production of North Atlantic deep water: sources, rates and pathways. *J Geophys Res* 99(C6):12319–12341
- Dobrolyubov SA (1991) Estimate of the freshwater component of meridional water transport in the ocean. *Meteorol Gidrol* 1:71–78
- Eliseev AV, Mokhov II (2003) Amplitude-phase characteristics of the annual cycle of surface air temperature in the Northern Hemisphere. *Adv Atmos Sci* 20(1):1–16
- England MH (1993) Representing the global-scale water masses in ocean general circulation models. *J Phys Oceanogr* 23:1523–1552
- Ewen TL, Weaver AJ, Eby M (2004) Sensitivity of the inorganic ocean carbon cycle to future warming in the UVic coupled model. *Atmos Ocean* 42:23–42
- Fichet T, Morales Maqueda MA (1997) Sensitivity of a global sea ice model to the treatment of ice thermodynamics and dynamics. *J Geophys Res* 102(C6):12609–12646

- Fiorino M (1997) A merged surface air temperature data set for the validation of AMIP I. PCMDI Web Rep, Lawrence Livermore National Laboratory [Available online at <http://www-pcmdi.llnl.gov/obs/ipcc/>]
- Gallée H, van Ypersele JP, Fichefet Th, Tricot Ch, Berger A (1991) Simulation of the Last Glacial Cycle by a Coupled, Sectorially Averaged Climate-Ice Sheet Model 1. The Climate Model. *J Geophys Res* 96(D7):13139–13161
- Ganachaud A, Wunsch C (2000) Improved estimates of global ocean circulation, heat transport and mixing from hydrographic data. *Nature* 408:453–457
- Ganopolski AV, Rahmstorf S, Petoukhov VK, Claussen M (1998) Simulation of modern and glacial climates with a coupled global model of intermediate complexity. *Nature* 391:351–356
- Ganopolski A, Petoukhov V, Rahmstorf S, Brovkin V, Claussen M, Eliseev A, Kubatzki C (2001) CLIMBER-2: a climate system model of intermediate complexity. Part II: Model sensitivity. *Clim Dyn* 17:735–751
- Gates WL, Mitchell JFB, Boer GJ, Cubasch U, Meleshko VP (1992) Climate modelling, climate prediction and model validation. In: Houghton JT, Callander BA, Varney SK (eds) *Climate change. The supplementary report to the IPCC Scientific Assessment*, Cambridge University Press, Cambridge, UK, pp 97–134
- Gates WL, Boyle JS, Covey C, Dease CG, Doutriaux CM, Drach RS, Fiorino M, Gleckler PJ, Hnilo JJ, Marlais SM, Phillips TJ, Potter GL, Santer BD, Sperber KR, Taylor KE, Williams DN (1999) An overview of the results of the Atmospheric Model Intercomparison Project (AMIP I). *Bull Amer Meteor Soc* 80(1):29–55
- Goody RM (1964) *Atmospheric radiation. I: Theoretical basis*. Clarendon Press, Oxford, 436 pp
- Goosse H, Renssen H (2001) A two-phase response of the Southern Ocean to an increase in greenhouse gas concentrations. *Geophys Res Lett* 28(18):3469–3472
- Goosse H, Selten FM, Haarsma RJ, Opsteegh JD (2001) Decadal variability in high northern latitudes as simulated by an intermediate-complexity climate model. *Ann Glaciol* 33:525–532
- Harrison EP, Minnis P, Barkstrom BP, Ramanathan V, Cess RD, Gibson GG (1990) Seasonal variation of cloud radiative forcing derived from the Earth Radiation Budget Experiment. *J Geophys Res* 95:18687–18703
- Harvey LDD (1992) A Two-Dimensional Ocean Model for long-term climate simulations: stability and coupling to Atmospheric Sea Ice Models. *J Geophys Res* 97(C6):9435–9453
- Hastenrath S (1982) On meridional heat transport in the world ocean. *J Phys Oceanogr* 12:922–927
- Holfort J (1994) *Grossräumige Zirkulation und meridionale Transporte im Südatlantik*. PhD Dissertation, Institut für Meereskunde, Kiel, Germany
- Hsiung J (1985) Estimates of global oceanic meridional heat transport. *J Phys Oceanogr* 15:1405–1413
- Hurrell JW, Campbell GG (1992) Monthly mean global satellite data sets available in CCM history tape format. NCAR Tech Note NCAR/TN-371+STR: 94 pp
- IPCC (1990) *Climate change: the IPCC scientific assessment*. In: Houghton JT, Jenkins GJ, Ephraums JJ (eds) Cambridge University Press, Cambridge, 365 pp
- IPCC (1995) *Climate Change 1995: the Science of climate change*. In: Houghton JT, Meira Filho LG, Callender BA, Harris N, Kattenberg A, Maskell K (eds) Cambridge University Press, Cambridge, 572 pp
- IPCC (2001) *Climate change 2001: the Scientific Basis*. In: Houghton JT, Ding Y, Griggs DJ, Noguer M, van der Linden PJ, Dai X, Maskell K, Johnson CA (eds) *Contribution of Working Group I to the Third Assessment Report of the Intergovernmental Panel on Climate Change*. Cambridge University Press, Cambridge, United Kingdom and New York, NY, USA, 881 pp
- Jäger L (1976) *Monatskarten des Niederschlags für die ganze Erde*. Ber Deutsche Wetterdienstes 18(139):38
- Jennings RL (1975) *Data sets for meteorological research*. NCAR Technical Note, NCAR-TN/1A, National Center for Atmospheric Research, Boulder, 156 pp
- Jones PD (1988) Hemispheric surface air temperature variations: recent trends and an update to 1987. *J Climate* 1:654–660
- Kalnay E, Kanamitsu M, Kistler R, Collins W, Deaven D, Gandin L, Iredel M, Saha S, White G, Woollen J, Zhu Y, Leetmaa A, Reynolds R, Chelliah M, Ebisuzaki W, Higgins W, Janowiak J, Mo KC, Ropelewski C, Wang J, Jenne R, Joseph D (1996) The NCEP/NCAR 40-year reanalysis project. *Bull Amer Met Soc* 77:437–471
- Kamenkovich I, Sokolov A, Stone P (2002) An efficient climate model with a 3D ocean and statistical-dynamical atmosphere. *Clim Dyn* 19:585–598
- Kessler A (1968) *Globalbilanzen von Klimatelementen. Ein Beitrag zur allgemeinen Klimatologie der Erde*. Ber. Inst Meteorol und Klimatol der Techn Univer Hannover No 3
- Kim S-J, Flato GM, Boer GJ, McFarlane NA (2002) A coupled climate model simulation of the Last Glacial Maximum, Part I: transient multi-decadal response. *Clim Dyn* 19:515–537
- Lambert SJ, Boer GJ (2001) CMIP1 evaluation and intercomparison of coupled climate models. *Clim Dyn* 17:83–106
- Le Treut H, McAvaney B (2000) A model intercomparison of equilibrium climate change in response to CO₂ doubling. Notes du Pôle de Modélisation de l'IPSL No 18, Institut Pierre Simon LaPlace, Paris, France
- Levermann A, Griesel A, Hofmann M, Montoya M, Rahmstorf S (2005) Dynamic sea level changes following changes in the thermohaline circulation. *Clim Dyn* 24:347–354
- Maier-Reimer E, Mikolajewicz U, Hasselmann K (1993) Mean circulation of the Hamburg LSG OGCM and its sensitivity to the thermohaline surface forcing. *J Phys Oceanogr* 23:731–757
- Manabe S, Stouffer RJ (1988) Two stable equilibria of a coupled ocean-atmosphere model. *J Climate* 1:841–866
- Manabe S, Stouffer RJ (1999) Are two modes of thermohaline circulation stable?. *Tellus* 51A:400–411
- Mann ME (1998) *A Study of Ocean-Atmosphere Interaction and Low-Frequency Variability of the Climate System*. PhD Thesis, Yale University, New Haven, CT, 283 pp
- Matthews HD, Weaver AJ, Eby M, Meissner KJ (2003) Radiative forcing of climate by historical land cover change. *Geophys Res Lett* 30(2):Art. No. 1055
- Meissner KJ, Weaver AJ, Matthews HD, and Cox PM (2003) The role of land-surface dynamics in glacial inception: A study with the UVic Earth System Model. *Clim Dyn* 21:515–537
- Mokhov II, Demchenko PF, Eliseev AV, Khon VCh, Khvorost'yanov DV (2002) Estimation of global and regional climate changes during the 19th–21st centuries on the basis of the IAP RAS model with consideration for anthropogenic forcing. *Izvestiya Atmos Ocean Phys* 38(5):555–568
- Mokhov II, Eliseev AV, Demchenko PF, Khon V Ch, Akperov MG, Arzahnov MM, Karpenko AA, Tikhonov VA, Chernokulsky AV, Sigaeva EV (2005) Climate changes and their assessment based on the IAP RAS global model simulations. *Doklady Earth Sci* (in press)
- Montoya M, Griesel A, Levermann A, Mignot J, Hofmann M, Ganopolski A, Rahmstorf S (2004) The Earth System Model of Intermediate Complexity CLIMBER-3 α . Part I: description and performance for present day conditions. *Clim Dyn* (in press)
- Oglesby RJ, Saltzman B (1990) Extending the EBMs—the effect of deep ocean temperature on climate with application to the cretaceous. *Glob Plan Change* 82(3–4):237–259
- Ohring G, Adler S (1978) Some experiments with a Zonally Averaged Climate Model. *J Atmos Sci* 35:186–205
- Oka A, Hasumi H, Sugimoto N (2001) Stabilization of thermohaline circulation by wind-driven and vertical diffusive salt transport. *Clim Dyn* 18:71–83
- Oort AH, Rasmusson EM (1971) *Atmospheric circulation statistics*. NOAA Prof Pap 5, Rockville: 323 pp
- Opsteegh JD, Haarsma RJ, Selten FM, Kattenberg A (1998) EC-BILT: a dynamic alternative to mixed boundary conditions in ocean models. *Tellus* 50A:348–367
- Peixoto JP, Oort AH (1983) *The atmospheric branch of the hydrological cycle and climate*. In: *Variations of the global water budget*. Reidel, London: 5–65

- Petoukhov VK (1980) A zonal climate model of heat and moisture exchange in the atmosphere over the underlying layers of ocean and land In: Golitsyn GS, Yaglom AM (eds) Physics of the atmosphere and the problem of climate. Moscow, Nauka: 8–41 (in Russian)
- Petoukhov VK (1991) Dynamical-statistical modeling of the large-scale climatic processes. Dr. habil. Thesis, Leningrad Hydrometeorological Institute, St. Petersburg, 431 pp (in Russian)
- Petoukhov VK, Mokhov II, Eliseev AV, Semenov VA (1998) The IAP RAS Global Climate Model. Dialogue Publishing House, Moscow State University, Moscow, 110 pp
- Petoukhov V, Ganopolski A, Brovkin V, Claussen M, Eliseev A, Kubatzki C, Rahmstorf S (2000) CLIMBER-2: A climate system model of intermediate complexity. Part I: Model description and performance for present climate. *Clim Dyn* 16:1–17
- Petoukhov V, Ganopolski A, Claussen M (2003) POTSDAM - a set of atmosphere statistical-dynamical models: theoretical background. PIK Report No 81, Potsdam Institute for Climate Impact Research (PIK), March 2003: 136 pp
- Petoukhov VK, Feygel'son YM (1973) A model of long-period heat and moisture exchange in the atmosphere over the ocean, *Izvestiya Atmos Ocean Phys* 9:352–362
- Prinn R, Jacoby H, Sokolov A, Wang C, Xiao X, Yang Z, Eckhaus R, Stone P, Ellerman D, Melillo J, Fitzmaurice J, Kicklighter D, Holian G, Liu Y (1999) Integrated global system model for climate policy assessment: feedbacks and sensitivity studies. *Clim Change* 41:469–546
- Rahmstorf S (1996) On the freshwater forcing and transport of the Atlantic thermohaline circulation. *Clim Dyn* 12:799–811
- Rahmstorf S, Ganopolski A (1999) Long-term global warming scenarios computed with an efficient coupled climate model. *Clim Change* 43(2):353–367
- Ramanathan V, Lian MS, Cess RD (1979) Increased atmospheric CO₂-zonal and seasonal estimates of the effect on the radiation energy-balance and surface-temperature. *J Geophys Res* 84(C8):4949–4958
- Renssen H, Goosse H, Fichefet T (2002) Modeling the effect of freshwater pulses on the early Holocene climate: The influence of high-frequency climate variability. *Paleoceanography* 17 (2), DOI 10.1029/2001PA000649
- Robock A (1980) The seasonal cycle of snow cover, sea ice and surface albedo. *Mon Wea Rev* 108:267–285
- Ropelewski CF (1989) Monitoring large-scale cryosphere/atmosphere interactions. *Adv Space Res* 9:213–218
- Rossov WB, Schiffer RA (1999) Advances in understanding clouds from ISCCP. *Bull Amer Meteor Soc* 80:2261–2287
- Rossov WB, Garder LC, Lu PJ, Walker AW (1991) International Satellite Cloud Climatology Project (ISCCP): documentation of cloud data. WMO/TD-No.266, World Meteorological Organization: 76 pp
- Saltzman B (1978) A Survey of Statistical-Dynamical Models of the Terrestrial Climate. *Advances in Geophysics* 20:183–295
- Saltzman B, Vernekar AD (1968) A parameterization of the large-scale transient eddy flux of relative angular momentum. *Mon Wea Rev* 96(12):854–857
- Saltzman B, Vernekar AD (1971) An equilibrium solution for the axially symmetric component of the earth's macroclimate. *J Geophys Res* 76(6):1498–1524
- Saltzman B, Vernekar AD (1972) Global Equilibrium Solutions for the Zonally Averaged Macroclimate. *J Geophys Res* 77(21):3936–3945
- Schiller A (1995) The mean circulation of the Atlantic Ocean north of 30S determined with the adjoint method applied to an ocean general circulation model. *J Mar Res* 53:453–497
- Schmittner A, Meissner KJ, Eby M, Weaver AJ (2002) Forcing of the deep ocean circulation in simulations of the Last Glacial Maximum. *Paleoceanogr* 17, 5:1–5:15 (10.1029/2001PA000633)
- Schmitz WJ (1995) On the interbasin-scale thermohaline circulation. *Rev Geophys* 33:151–173
- Schmitz Jr W, McCartney MS (1993) On the North Atlantic circulation. *Rev Geophys* 13:29–49
- Schubert S, Wu C-Y, Zero J, Schemm J-K, Park C-K, Suarez M (1992) Monthly means of selected climate variables for 1985–1989. NASA Techn Memo, Goddard Space Flight Center: 376 pp
- da Silva AM, Young CC, Levitus S (1994) Atlas of Surface Marine Data, Vol 2: Anomalies of Directly Observed Quantities. NOAA Atlas NESDIS 7, U.S. Department of Commerce, Washington DC: 416 pp
- Stocker TF, Wright DG, Mysak LA (1992) A zonally averaged, coupled ocean-atmosphere model for paleoclimate studies. *J Climate* 5:773–797
- Stone PH (1972) A Simplified Radiative-Dynamical Model for the Static Stability of Rotating Atmospheres. *J Atmos Sci* 29 (3):405–418
- Stowe LL, Jacobowitz H, Ohring G, Knapp KR, Nalli NR (2002) The Advanced Very High Resolution Radiometer (AVHRR) Pathfinder Atmosphere (PATMOS) climate dataset: Initial analysis and Evaluation. *J Climate* 15:1243–1260
- Talley LD (1984) Meridional heat transport in the Pacific Ocean. *J Phys Oceanogr* 14:231–241
- Talley LD, Reid JL, Robbins PE (2003) Data-based meridional overturning streamfunction for the Global Ocean. *J Climate* 16:3213–3226
- Trenberth KE, Solomon A (1994) The global heat balance: heat transport in the atmosphere and ocean. *Clim Dyn* 10:107–134
- Verbitsky MYa, Chalikov DV (1986) Modelling of the Glaciers-Ocean- Atmosphere System. In: Monin AS (ed) Leningrad, Hydrometeoizdat, 133 pp. (in Russian)
- Wang Z, Mysak LA (2000) A simple coupled atmosphere-ocean-sea ice-land surface model for climate and paleoclimate studies. *J Climate* 13:1150–1172
- Wang Z, Mysak LA (2002) Simulation of the last glacial inception and rapid ice sheet growth in the McGill Paleoclimate Model. *Geophys Res Lett*, 29(23), 10.1029/2002GL015120
- Warren SG, Hahn CJ, London J, Chervin RM, Jenne RL (1986) Global distribution of total cloud cover and cloud type amounts over the ocean. Technical note tn-273 + strNCAR-Boulder, CO42pp. + 185 maps
- Warren SG, Hahn CJ, London J, Chervin RM, Jenne RL (1988) Global distribution of total cloud cover and cloud type amounts over land. Technical note tn-273 + strNCAR-Boulder, CO42pp. + 200 maps
- Weaver AJ, Eby M, Fanning AF, Wiebe EC (1998) Simulated influence of carbon dioxide, orbital forcing and ice sheets on the climate of the last glacial maximum. *Nature* 394:847–853
- Weaver AJ, Eby M, Wiebe EC, Bitz CM, Duffy PB, Ewen TL, Fanning AF, Holland MM, MacFadyen A, Matthews HD, Meissner KJ, Saenko O, Schmittner A, Wang HX, Yoshimori M (2001) The UVic Earth System Climate Model: model description, climatology, and applications to past and future climates. *Atmosphere-Ocean* 39(4):361–428
- Xie P, Arkin P (1997) Global precipitation: A 17-year monthly analysis based on gauge observations, satellite estimates, and numerical model outputs. *Bull Amer Meteor Soc* 78:2539–2558
- Zebiak SE, Cane MA (1987) A Model El Niño-Southern Oscillation. *Mon Wea Rev* 115:2262–2278